Brachinites – igneous rocks from a differentiated asteroid

David W. Mittlefehldt[1], Donald D. Bogard[1], John L. Berkley[2] and Daniel H. Garrison[3]

[1]mail code SR, NASA/Johnson Space Center, Houston, TX 77058, USA

[2]Dept. of Geosciences, SUNY College at Fredonia, Fredonia, NY 14063, USA

[3]C23, Lockheed Martin SO, 2400 Nasa Rd. 1, Houston, TX 77058, USA

corresponding author's e-mail: david.w.mittlefehldt@nasa.gov

Meteoritics & Planetary Science
submitted: 24 February 2003
revised: 27 August 2003

Abstract ¾ We have done petrologic studies of brachinites ALH 84025, EET 99402 and EET 99407, bulk geochemical studies of EET 99402 and EET 99407, Ar-Ar studies of Brachina and EET 99402 and a Xe isotopic study of Brachina. Textural, mineral compositional and bulk compositional evidence show that EET 99402 and EET 99407 are paired. ALH 84025, EET 99402 and EET 99407 have igneous textures. Petrofabric analyses of ALH 84025 and EET 99407 demonstrate the presence of lineations and probable foliations of olivine grains that support formation as igneous cumulates. Mineral minor element chemistry and bulk rock incompatible lithophile element contents of the brachinites are distinct from those of acapulcoite-lodranite clan meteorites, a suite of high-grade metamorphic rocks and anatectic residues. The differences demonstrate a higher blocking temperature of equilibration for the brachinites, and that cumulus plagioclase is present in EET 9940n and probably ALH 84025, thus indicating an igneous origin. Brachinites are differentiated, ultramafic achondrites, not part of a suite of primitive achondrites, and we infer that their parent asteroid is a differentiated body.

Brachina has an excess of ^{129}Xe correlated with reactor-produced ^{128}Xe demonstrating that short-lived ^{129}I was present at the time of formation. This, plus literature data, attest to early formation of the brachinites, within a few Ma of the formation of chondrites. Argon-Ar age studies show that Brachina and EET 99407 were degassed about 4.13 Ga ago, possibly by a common impact event. EET 9940n show petrographic evidence for shock, including possible conversion of plagioclase to maskelynite followed by devitrification. Brachina is unshocked, making a direct association between the Ar-Ar age and textures ambiguous.

INTRODUCTION

The brachinite group of meteorites is small and incompletely studied. There are ten brachinites, but pairing reduces the number of true individuals to at most eight. Including this study, only half of them have been subjected to detailed study – the rest are described only in abstracts, the *Catalogue of Meteorites* or *The Meteoritical Bulletin*. Mittlefehldt (2003) and Mittlefehldt et al. (1998) summarized the petrology, chemistry and chronology of the group. Brachinites exhibit a somewhat diverse petrology, but all are composed dominantly of olivine - 79 to 93% - and all contain high-Ca pyroxene. All but three contain plagioclase, and all but four contain orthopyroxene. Chromite and Fe-sulfide are minor components reported in most brachinites, and metal and phosphates are trace components in several. Table 1 summarizes the petrology of brachinites.

Compositional information is available only for ALH 84025, Brachina and Eagles Nest, but the data for Eagles Nest indicate substantial terrestrial contamination (Johnson et al., 1977; Nehru et al., 1983; Swindle et al., 1998; Warren and Kallemeyn, 1989). ALH 84025 and Brachina differ significantly in bulk composition – Brachina has nearly chondritic abundances of incompatible lithophile elements, whereas ALH 84025 is depleted (Johnson et al., 1977; Nehru et al., 1983; Warren and Kallemeyn, 1989). Siderophile element abundance patterns are variable, but brachinites are depleted in these elements by factors of ~0.1 to 0.7 compared to CI chondrites (Nehru et al., 1983; Swindle et al., 1998; Warren and Kallemeyn, 1989). Noble gas data for ALH 84025 and Brachina show that they have relatively high trapped noble gas contents, with $^{36}Ar_{trapped}$ of 2.1×10^{-8} and 0.82×10^{-8} cm^3 g^{-1}, respectively (Ott et al., 1985; 1987).

Very few chronological studies have been done on brachinites, much of it published only in abstracts, but the data are sufficient to show that the brachinites were formed early in solar system history. Brachina, ALH 84025 and Eagles Nest contain excess ^{129}Xe from in-situ decay of ^{129}I ($t_{½}$ 17 Ma) (Bogard et al., 1983; Ott et al., 1987; Swindle et al., 1998). Bogard et al. (1983) noted that the Brachina data indicate that retention of ^{129}Xe began no later than 4.4 Ga ago, and Swindle et al. (1998) concluded that Eagles Nest began retaining ^{129}Xe within ~50 Ma of primitive chondrites. Crozaz and Pellas (1984) studied particle tracks in phosphate, high-Ca pyroxene and olivine grains from Brachina, and concluded that fission tracks from ^{244}Pu ($t_{½}$ 82 Ma) are present and that track retention began ~4.5 Ga ago. Wadhwa et al. (1998a) found

excesses in ^{53}Cr correlated with the Mn/Cr ratio indicating that ^{53}Mn ($t_{½}$ 3.7 Ma) was present in Brachina. They calculated a formation age of 4.5637±0.0009 Ga through comparison with the $^{53}Mn/^{55}Mn$ ratio and Pb-Pb age of angrite LEW 86010. They noted that Brachina was at most only ~5 Ma younger than the oldest known objects from the solar system - CAIs from Allende.

Nehru et al. (1992) classified brachinites as primitive achondrites, but recent studies have rather supported a cumulate origin for ALH 84025, Eagles Nest, EET 99402 and EET 99407 (Mittlefehldt and Berkley, 2002; Swindle et al., 1998; Warren and Kallemeyn, 1989). We consider primitive achondrites to be those with metamorphic textures and lithophile, siderophile and chalcophile element contents similar to the ranges exhibited by nebular materials. Some individual members may show somewhat fractionated element patterns, but unfractionated members dominate primitive achondrite groups. The acapulcoite-lodranite clan is the archetype primitive achondrite group, and will be used here to contrast brachinite properties to those expected of primitive achondrites. In contrast, differentiated achondrites exhibit igneous textures, possibly modified by impact and/or thermal metamorphism, and have lithophile, siderophile and chalcophile element contents that are highly fractionated from the ranges of nebular materials.

Here we report on our completed petrologic studies of ALH 84025, EET 99402 and EET 99407, bulk compositional studies of EET 99402 and EET 99407, Ar-Ar studies of Brachina and EET 99402, and Xe isotopic study of Brachina. EET 99402 and EET 99407 were believed to be paired based on preliminary characterization, and we confirm here that they are. We will refer to the pair as EET 9940n for convenience. We use our data on EET 9940n to determine the petrogenesis and thermal history of this brachinite, and then discuss the origin of the group using all available data. In particular, we wish to address the question of whether brachinites are primitive or differentiated achondrites.

SAMPLES AND ANALYTICAL METHODS

We obtained polished thin sections of ALH 84025, EET 99402 and EET 99407 for petrographic observation and electron microprobe analysis (EMPA) from NASA Johnson Space Center (JSC). We did EMPA using the Cameca SX100 electron microprobe at NASA JSC.

Analytical conditions were 20 kV, 40 nA, 1 μm beam for mafic silicates, oxides, metal and troilite, and 15 kV, 20 nA, 10×10 μm rastered beam for plagioclase.

We made digital x-ray maps on the SX100 electron microprobe for the elements Mg, Al, Si, P, S, Ca, and Fe at a point spacing of 10 μm. Total areas covered (after subtraction of regions of epoxy) were 0.187 cm^2 for ALH 84025,6, 0.241 cm^2 for ALH 84025,26 and 0.478 cm^2 for EET 99402,22. Our bulk rock data and thin section examination showed that EET 99402 and EET 99407 have very similar modal mineral abundances, hence we did x-ray mapping only of one. Warren and Kallemeyn (1989) noted that different thin sections of ALH 84025 are distinct. Thus, we did x-ray mapping of one from each potted butt used to make thin sections. The data arrays (x-y coordinates plus x-ray intensities) were manipulated with the Interactive Data Language of Research Systems, Inc. X-ray intensity filters were defined for each mineral, and x-ray intensities were then used to identify the phase at each x,y position. These were then converted to modal abundances for each thin section.

We obtained two interior chips of EET 99402 (490 and 650 mg) and one of EET 99407 (540 mg) from NASA JSC for instrumental neutron activation analysis (INAA). Each sample was ground, homogenized and split to yield ~50 mg for INAA. The INAA was done using standard JSC procedures (Mittlefehldt, 1994). The samples, standards and controls were sealed in pure silica glass tubes and irradiated at the University of Missouri Research Reactor Facility for 24 hours at a flux of 5.5×10^{13} n cm^{-2} sec^{-1}. The samples were counted four times roughly ¾, 1, 5 and 15 weeks after irradiation to obtain data for nuclides of differing half-lives.

We obtained an interior chip of Brachina from the American Museum of Natural History (AMNH #4489E), and an interior chip of EET 99402 (,20) from NASA JSC for Ar-Ar and noble gas analyses. A 47 mg sample of EET 99402 was irradiated in the University of Missouri Research Reactor Facility, along with several samples of hornblende NL-25, which is used as a flux and age monitor (Bogard et al, 1995). Irradiation converts a portion of the ^{39}K to ^{39}Ar via (n,p) reaction, which then resides in the same lattice sites as ^{40}Ar from natural decay of ^{40}K. A portion of the ^{40}Ca is also converted to ^{37}Ar via (n,a) reaction. Argon was extracted by stepwise temperature release and its isotopic composition was analyzed on a VG-3600 mass spectrometer. A 199 mg split of the Brachina sample crushed to <100 mesh was used for Ar-Ar analysis. It and samples of NL-25 hornblende were irradiated in 1982 at the Brookhaven National

Laboratory, and extracted Ar was analyzed on a Nuclide 6-60 mass spectrometer. Irradiation constants (J values) for the irradiations were 0.02265±0.0001 (UM) and 0.1030±0.0006 (BNL). Because of the moderately high K content of the Brachina sample, blanks and reactor-produced interferences on ^{39}Ar were not significant. Because of the very low K concentration of our EET 99402 sample, corrections applied for blanks and reactor-produced interferences on ^{39}Ar were generally significant - they ranged from <1% to ~3%. Blank corrections to ^{40}Ar for those extractions primarily used to deduce an age ranged from ~2 to 15%, whereas corrections to extractions releasing smaller ^{40}Ar concentrations were larger. Corrections for ^{39}Ar produced in the reactor from Ca were <10% for most extractions, but were higher for those extractions releasing the last 4% of the total ^{39}Ar. Through multiple measurements on irradiated CaF, we have defined the uncertainty in these reactor corrections to <2-3%. Uncertainties shown for calculated Ar-Ar ages of individual extractions incorporate uncertainties in blank, reactor, and decay corrections, but not uncertainties in the irradiation constant (J value) or the hornblende monitor age (=0.5%). However, where we give an average age for several extractions, the uncertainty in this "plateau" age does include the uncertainty in J. We assigned an uncertainty to each blank correction equal to the correction itself, although we believe that the blanks are known more accurately than this. Preliminary data for Brachina were reported by Bogard et al. (1983).

RESULTS

General Petrography and Mineral Chemistry

We have done detailed petrographic and mineral compositional studies of ALH 84025, EET 99402 and EET 99407. EET 9940n (EET 99402 and EET 99407 are identical) is a coarse grained rock with overall xenomorphic-granular texture composed of olivine, high-Ca pyroxene, plagioclase, Cr-rich spinel, iron sulfide and rare metal (Fig. 1). Olivine generally occurs as equant grains ~0.5-1.5 mm across, although prismatic grains are also present. Some of the larger olivine grains have irregular margins, with deep embayments. Olivine grains are often joined at triple junctures, commonly show undulatory extinction, and contain planar fractures. High-Ca pyroxene occurs as roughly equant to irregular grains 0.2-0.7 mm across, is often interstitial to olivine, and is commonly twinned. Some high-Ca pyroxene grains partially to completely enclose olivine grains. Plagioclase occurs as highly irregular interstitial patches 0.2-1.5 mm

across. These patches are composed of mosaics of numerous tiny grains, commonly contain vesicles up to 100 μm across, and often partially or entirely enclose olivine grains. Spinel occurs as equant to irregular, interstitial grains ~0.02-0.3 mm across. Sulfide and rare metal occur as generally <10 μm grains forming abundant curvilinear inclusion surfaces in all other phases. This gives EET 9940n a dark, dusty appearance in transmitted light (Fig. 1). We used our INAA data for Na, Ca, Cr and Se (assuming a chondritic S/Se ratio), and mineral composition data, to estimate the weight percentages of minerals in EET 9940n – olivine 88.2%, high-Ca pyroxene 4.1%, plagioclase 5.4%, spinel 1.0%, and troilite 1.3%. This compares well with the mineral mode determined by x-ray mapping of EET 99402 (Table 1) when converted to weight percent - olivine 88.0%, high-Ca pyroxene 4.7%, plagioclase 6.1%, spinel 1.0%, and troilite 0.1%. Based on deformation textures of olivine, we estimate a shock stage of S3 using the ordinary chondrite shock stage classification (Stöffler et al., 1991). Weathering appears restricted to minor iron oxide staining along grain boundaries, and suggests a weathering category of W0-W1 (Wlotzka, 1993). However, because metal and sulfides in these meteorites are mostly tiny grains enclosed in host silicate and oxide grains, this scale, devised for metal- and troilite-rich ordinary chondrites, may not be appropriate.

Mason et al. (1992) and Warren and Kallemeyn (1989) have described the texture of ALH 84025, and we will only contrast ALH 84025 with EET 9940n. Although olivine and high-Ca pyroxene in ALH 84025 also contain tiny (most <15 μm) metal, troilite and chromite inclusions, they are much less abundant than the ubiquitous inclusions typical of EET 9940n, making ALH 84025 much more transparent in thin section (Fig. 1). In addition, metal and troilite occur in part as relatively large grains in ALH 84025, up to 1.6 mm for troilite and 0.4 mm for metal (Warren and Kallemeyn, 1989), unlike EET 9940n. The mineral modes of the two ALH 84025 thin sections agree well with each other - the major difference is antithetic variation in olivine and high-Ca pyroxene (Table 1). Our modes also agree with the range of modes given by Warren and Kallemeyn (1989). Olivine shows only mild undulatory extinction and few, if any, planar fractures, indicating a shock stage of S2 (Stöffler et al., 1991). Weathering appears restricted to minor iron oxide staining along grain boundaries, and suggests a weathering category of W0-W1 (Wlotzka, 1993). Because many metal and troilite grains are large and not enclosed in silicate grains, the weathering scale developed for ordinary chondrites is applicable to ALH 84025.

The minerals in ALH 84025 and EET 9940n are uniform in composition. Those of EET 99402 and EET 99407 are identical, supporting pairing of these stones. Representative grain compositions are given in Tables 2-4. Olivine in EET 9940n has an average composition of $Fo_{64.2}$, with molar Fe/Mn of 76.2. For ALH 84025, olivine compositions average $Fo_{66.5}$, with molar Fe/Mn of 68.3. Olivine has relatively high CaO contents, averaging 0.12 wt% for EET 9940n and 0.10 wt% for ALH 84025, as is typical of brachinites (e.g., see Warren and Kallemeyn, 1989). Brachinites are distinct from primitive achondrites such as the acapulcoite-lodranite clan, or equilibrated chondrites in this (Fig. 2). The NiO contents are close to the detection limit, and slightly less than found for Brachina (0.014-0.020 vs. ~0.045, Table 2, Smith et al., 1983). However, one region of an otherwise typical olivine grain in ALH 84025 has elevated NiO contents (Table 2).

High-Ca pyroxene in EET 9940n is diopside with an average composition of $Wo_{46.0}En_{43.7}Fs_{10.3}$ with molar Fe/Mn of 40.1. High-Ca pyroxene in ALH 84025 is augite with an average composition of $Wo_{43.4}En_{45.4}Fs_{11.2}$ with molar Fe/Mn of 31.5. High-Ca pyroxene is Na- and Ti-poor compared to those of primitive achondrites and equilibrated ordinary chondrites, and at the low end of their range for Cr (Fig. 3).

We determined plagioclase compositions only for EET 99407. The plagioclase patches are composed of masses of grains a few microns in size, thus the 10×10 μm rastered beam analyses are not of individual grains. Further, x-ray mapping of one of the plagioclase patches shows the presence of a few ~5 μm-size grains with differing Ca/Na. With these caveats in mind, we found that the average plagioclase composition is $An_{39.7}Ab_{60.1}Or_{0.2}$. (The end-member composition reported by Mittlefehldt and Berkley (2002) is incorrect due to computational error.) This plagioclase is Ca-rich and very K-poor compared to those of primitive achondrites, equilibrated ordinary chondrites and Brachina (Fig. 4). Plagioclase is absent in ALH 84025 (Table 1; Warren and Kallemeyn, 1989).

Chrome-rich spinel in ALH 84025 is within the range of compositions of primitive achondrite spinels, and is Ti-poor compared to those of equilibrated ordinary chondrites (Fig. 5) Spinel grains in EET 9940n are distinct. They have higher Al contents (13.5 wt% Al_2O_3 vs. 7.5 wt%), and much lower Zn contents (=0.03 wt% ZnO vs. 0.44 wt%). However, one euhedral spinel grain enclosed in plagioclase in EET 99407 has a ZnO content of 0.40 wt%, like those of

ALH 84025. This grain has a slightly higher mg#, but is otherwise unexceptional (Table 3). The ZnO contents of spinels in ALH 84025 are at the low end of the range for acapulcoite-lodranite clan meteorites, and slightly above the range for the L7 chondrite LEW 88663 (Fig. 5).

Troilite and the rare metal grains in EET 9940n were not analyzed due to their small size. Metal in ALH 84025 is taenite with four grains yielding a range of 28.9-31.4 wt% Ni and 1.58-1.67 wt% Co. Three of the grains have essentially identical Co/Ni atom ratios of 0.053, while the other has a ratio of 0.056. Four troilite grains have Ni contents in the range 0.42-0.62 wt%, and Co contents of 0.06 wt%. An exceptional grain contains 0.04 wt% Ni and 0.03 wt% Co.

Petrofabric Analysis

Many olivine grains in thin section of EET 99407,9 have very similar birefringence, possibly indicating similar crystallographic orientation. Warren and Kallemeyn (1989) noted that prismatic olivine grains in part of thin section ALH 84025,7 appeared to show preferred orientation. To aid in understanding of the physical processes involved in brachinite formation, we performed universal stage petrofabric analyses on olivine grains in polished thin sections EET 99407,9 and ALH 84025,6 - a serial section from the same potted butt as ALH 84025,7. The orientations of X (fast), Y (intermediate), and Z (slow) light vibration axes were plotted on a Schmidt equal area stereonet and the points contoured using a Kalsbeek counting net (Fig. 6). Because olivine crystallographic axes are parallel to light vibration axes, the plots show the corresponding a, b, and c crystallographic axes directly. Of particular interest are the Y=c axes because they represent the long axes of ideal olivine crystals.

EET 99407,9 shows no obvious visual indication of olivine or pyroxene preferred orientation - lineation or foliation textures are absent. However, the olivine c axes (Y) are highly concentrated in or near the center of the stereonet indicating many are oriented nearly perpendicular to the thin section plane (Fig. 6a). Maximum concentration is 14% in 1% of area (that is, 14 times the concentration expected for a random distribution), with a secondary high concentration (10% in 1% of area) oriented nearly in the plane of the thin section and trending NW-SE in Fig. 6a. ("North" is equated with the tops of the stereonets.) The prevalence of vertical c axes (with a fairly high degree of scatter otherwise) explains why a visible lineation is not apparent in EET 99407,9 – the long axes of many grains are perpendicular to the thin section

plane. Most grains display nearly equidimensional basal sections, or otherwise show no obvious preferred orientation.

Scrutiny of the overall patterns of all three crystallographic axes is required to ascertain whether a foliation exists. Ideal olivine crystals, particularly those of igneous origin, commonly show a broad (010) face, so that olivine foliations tend to consist of quasi-parallel (010) faces (Brothers, 1964). This foliation should show rotation around the X=b axis [010] with parallel or sub-parallel Y=c and Z=a girdle bands. That pattern is absent in EET 99407, however parallel X=b and Y=c girdles (NE-SW) do occur, rotating about a stable Z=a axis (NW-SE; Fig. 6a). Thus, if a foliation exists in EET 99407, it consists of parallel (100) faces; not (010) faces. In addition, high concentrations of essentially horizontal X=b and Y=c axes trending NW-SE suggest that another foliation may crisscross the NE-SW foliation. These relationships suggest that olivine grains, although displaying some remarkable preferred orientations, do not conform to a well-defined, easily explained orientation model.

ALH 84025,6 has a weak, but visible lineation as observed by Warren and Kallemeyn (1989) in parallel thin section ,7. The lineation was oriented horizontally (E-W) for petrofabric measurement (Fig. 6b). Olivine Y=c shows a strong east-dipping, E-W horizontal trend but with a maximum concentration of only about half that of EET 99407 (8% in 1% of area; Fig. 6b). Both X and Z also show fairly strong maxima (both also 8%) and like Y, show considerable variation as well. Both Y=c and Z=a show a tendency to plot near the margins (horizontal) of stereonets, with X=b concentrated near the center. This relationship suggests the existence of a (010) face foliation as described above roughly parallel to the thin section plane. The Y=c lineation is contained within that foliation, plunging somewhat to the east (Fig. 6b).

To test the idea that the visual lineation corresponds directly to the Y=c measured lineation, we performed a separate U-stage analysis of elongate grains (high aspect ratio; Fig. 7a) versus equant olivine grains (low aspect ratio; Fig. 7b). The objectives were to determine the extent to which elongate grains are contributing to the overall orientation pattern, particularly to the lineation maximum (Y=c), and to evaluate the contribution of equant olivine grains to the pattern to see if they represented a distinct orientation set.

Surprisingly, the two sets of olivine orientation patterns - elongate versus equant - are nearly identical (Fig. 7). Equant grains show a more pronounced tendency for Z axes to

concentrate around the periphery of the stereonet (horizontal), although in general terms the diagrams for both grain types are similar. This shows that equant grains are affected by the same mechanical processes during crystallization as the elongate grains. This relationship shows that the visual lineation does not do justice to the true magnitude of the preferred orientation of olivine grains in ALH 84025.

Geochemistry

We have done INAA on two samples of EET 99402 and one of EET 99407 (Table 5). Our INAA procedure does not allow determination of Mg, Al and Si, but we have estimated these for the samples using mineral compositions and abundances calculated as described above. There is some circularity in these calculations, but the calculated contents should be close to true values. We have also calculated the major element composition of EET 99402 from the mineral mode (Table 1). The bulk rock compositions of EET 99402 and EET 99407 are identical in nearly all elements measured, and quite distinct from the other brachinites. In some cases, differences between the two splits of EET 99402 are as large or larger than the differences between them and EET 99407. Thus, the small differences in composition between EET 99402 and EET 99407 do not negate pairing for these two stones.

EET 9940n is highly depleted in incompatible lithophile elements. A 2s upper limit for La is more than a factor of 3 lower than the La content of ALH 84025, but EET 9940n has a much higher Eu/Sm ratio (Fig. 8). EET 9940n is distinct from basalt-depleted primitive achondrites, the lodranites, in that the latter more typically show depletions in Eu relative to Sm, and none show REE depletions as great as those of EET 9940n. With the exception of Co, EET 9940n has a greater depletion in siderophile elements and Se than the other brachinites (Fig. 9).

Argon-Ar and Xe Isotopes

Our sample of EET 99402 had a K concentration of only 31 µg/g, whereas our Brachina sample contained 230 µg/g. Potassium is expected to reside primarily in minor plagioclase. The plagioclase modal abundance is lower in EET 99402 than Brachina (Table 1), and its K_2O content is 0.038 wt% for EET 99407 (Table 2) compared to 0.26 wt% for Brachina (Nehru et al., 1983). The spectra of ^{39}Ar-^{40}Ar ages and K/Ca ratios as a function of cumulative release of ^{39}Ar for EET 99402 are shown in Fig. 10. Steps in the age spectrum and K/Ca ratio, as well as some other characteristics of the Ar release data, suggest the existence of three K-bearing “phases,”

possessing slightly different Ar compositions and diffusion properties. These are changes in the relative rate of release of ^{39}Ar, and the $^{36}Ar/^{37}Ar$ and $^{36}Ar/^{38}Ar$ ratios as a function of extraction temperature. Those extractions releasing 0-13% of the total ^{39}Ar show relatively high and decreasing $^{36}Ar/^{37}Ar$ and $^{36}Ar/^{38}Ar$ ratios, lower Ar-Ar ages, and high K/Ca ratios. These are all consistent with adsorbed terrestrial Ar and loss of radiogenic ^{40}Ar, probably caused by weathering. (See Garrison et al. (2000) for a discussion of how Ar isotopic ratios can be used to identify Ar components.) Thus, we conclude that the younger Ar ages for the first ~13% of the ^{39}Ar release reflect diffusive loss of ^{40}Ar during antarctic weathering of feldspar grain surfaces.

The next eight extractions, releasing ~13-49% of the ^{39}Ar, show a constant K/Ca ratio, nearly constant $^{36}Ar/^{38}Ar$ ratios indicative of only cosmogenic Ar, and have the same Ar-Ar age within their respective uncertainties. The average age of these eight extractions is 4.13±0.06 Ga. The next three extractions, releasing ~49-99% of the ^{39}Ar in a separate release peak, also have a common age within their uncertainties, whose average value is 4.265±0.025 Ga. Increases in $^{36}Ar/^{38}Ar$ and $^{36}Ar/^{37}Ar$ ratios for these extractions indicate release of ~2.6×10^{-8} cm^3 g^{-1} of trapped, meteoritic ^{36}Ar, an amount similar to that contained in ordinary chondrites. We interpret the two different age plateaus for EET 99402 to indicate different degrees of ^{40}Ar degassing from phases with different Ar degassing properties. With the reasonable assumption that the phase releasing ~13-49% of the ^{39}Ar was totally degassed by the heating event, this event occurred 4.13±0.06 Ga ago.

The Ar-Ar age spectrum for Brachina (Fig. 11) is more difficult to interpret, but reveals some characteristics similar to those of EET 99402. The $^{36,37,38}Ar$ data indicate that significant amounts of terrestrial Ar were released in the first few extractions (0-17% ^{39}Ar release). The younger ages for these extractions were likely produced by terrestrial weathering, and possibly compounded by prior crushing of the sample. Either atmospheric or trapped meteoritic ^{36}Ar also seems to have been released over ~17-30% ^{39}Ar release. The average age for eleven extractions releasing 30-100% of the ^{39}Ar is 4.25±0.06 Ga. The reason for the decrease in age at ~55% ^{39}Ar release (Fig. 11) is not apparent, as the steady decrease in K/Ca seems inconsistent with a ^{39}Ar recoil effect. This age minimum, 4.13 Ga, is identical to the inferred degassing age of EET 99402. The age spectrum over 20-100% ^{39}Ar release may represent separate partial ^{40}Ar diffusion loss profiles from phases with different Ar diffusion properties, as suggested for EET

99402. A $^{40}Ar/^{36}Ar$ versus $^{39}Ar/^{36}Ar$ isochron plot of those extractions releasing 30-100% of the ^{39}Ar is linear (R^2 =0.9994) and gives an age of 4.28±0.02 Ga and a $^{40}Ar/^{36}Ar$ intercept of –151±179. However, the possible negative intercept suggests that this may be a false isochron produced by different degassing rates between $^{39,40}Ar$ produced from K and cosmogenic ^{36}Ar (Bogard and Garrison, 2003).

We also measured the Xe isotopic composition of the irradiated Brachina sample. For extractions 425-1075°C, we combined Xe across two consecutive extractions before making Xe isotopic measurements. Our Brachina sample contained significant amounts (~3×10^{-10} cm^3 g^{-1}) of excess ^{129}Xe from the decay of extinct ($t_{½}$ 17 Ma) ^{129}I, along with quantities of ^{128}Xe produced from ^{127}I during the irradiation. Figure 12 plots measured $^{129}Xe/^{132}Xe$ ratios versus $^{128}Xe/^{132}Xe$ ratios. Five high temperature extractions (1125-1500°C) released 57% of the total ^{128}Xe and show a strong linear correlation (R^2=0.9997). The trend line defined by these five extractions suggests a trapped $^{129}Xe/^{128}Xe$ ratio of 0.69, slightly lower than the terrestrial value. These five high temperature extractions also released ~50% of the ^{39}Ar (Fig. 11). This linear correlation demonstrates that much of the I-Xe system was not disturbed by the heating event that affected the K-Ar system. In contrast, the 300-1075°C extractions all show diffusive loss of ^{129}Xe relative to the linear correlation of high temperature data, consistent with loss of ^{40}Ar as observed for some of these extractions. Because we did not include an I-Xe age monitor in the irradiation, we cannot calculate an age from these data.

We can compare our noble gas results for EET 99402 and Brachina with those obtained for other brachinites. The only other reported Ar-Ar age study for a brachinite is for Eagles Nest (Swindle et al., 1998). The overwhelming majority of the ^{40}Ar was released at relatively low extraction temperatures and was attributed by the authors to terrestrial Ar contamination in this weathered australian find. Intermediate extraction temperatures show ages of ~0.7 Ga, which rise to ages of ~3.9-4.8 Ga at higher extraction temperatures. Although these data may indicate strong degassing of Eagles Nest prior to its fall to Earth, errors in the individual Ar ages are large, and it is conceivable that terrestrial weathering produced part of the loss of radiogenic ^{40}Ar. Eagles Nest contains ~1.8 x10^{-10} cm^3 g^{-1} excess ^{129}Xe, but this does not correlate with I, suggesting a disturbance of the I-Xe system (Swindle et al., 1998). ALH 84025 also contains an

amount of excess ^{129}Xe (1.9×10^{-10} cm^3 g^{-1}) similar to that in Brachina and Eagles Nest, and an amount of trapped ^{36}Ar (2.1×10^{-8} cm^3 g^{-1}) similar to that in EET 99402 (Ott et al., 1987).

DISCUSSION

Our understanding of the nature and origin of brachinites is evolving. Based on mineralogy, texture and bulk composition, Brachina was originally thought to be an igneous rock that crystallized from a melt of its own composition (Johnson et al., 1977). Floran et al. (1978) agreed that Brachina is an igneous rock, but they preferred a cumulate rather than a crystallized melt origin. Ryder (1982) suggested that Brachina is an impact-melt. This hypothesis was developed to explain how Brachina could be related to some martian meteorites in spite of distinctive oxygen isotopic composition and siderophile element contents. Ryder pointed out that the textural characteristics of Brachina are consistent with an impact-melt origin. Finally, Nehru et al. (1983) concluded that Brachina was a primitive achondrite, although they acknowledged that it lost a sulfide component through melting, contained essentially no metal, may have reached incipient melting of the silicate system, and has an igneous texture. They also suggested that Brachina might be related to a primitive achondrite super-group including the acapulcoites, lodranites, winonaites and silicate inclusions in IAB and IIICD irons.

Brachinites described since this early work have been interpreted as being igneous in origin. Warren and Kallemeyn (1989) argued that the texture, including a possible fabric, and the incompatible lithophile element contents of ALH 84025 demonstrate a cumulate origin for this rock. They further argued that a cumulate origin for ALH 84025 made it more plausible that Brachina is also a cumulate. Similarly, Swindle et al. (1998) argued that the texture of Eagles Nest indicates a cumulate origin. Because of terrestrial contamination, the incompatible lithophile element contents of Eagles Nest do not provide a strong constraint on its origin, but Swindle et al. (1998) stated that the bulk composition of Eagles Nest is consistent with a cumulate origin.

In stark contrast, Nehru et al. (1996) extended their earlier model by noting that some brachinites are depleted in a basaltic component, while others are not. They suggested that brachinites are therefore a direct analog to the acapulcoite-lodranite clan. They posited that brachinites were formed by a sequence of heating and oxidation of primitive chondritic material.

Oxidation converted most Fe metal to FeO forming olivine at the expense of orthopyroxene, and some regions reached the solidus temperature forming basaltic melt which was expelled from the solid residue (Nehru et al., 1996).

Thus, the major competing hypotheses for brachinite origin currently are; (i) metamorphism and oxidation of chondritic material, including anatexis for some (Nehru et al., 1983, 1996), or (ii) accumulation from a magma (Swindle et al., 1998; Warren and Kallemeyn, 1989). The first order question for our discussion, then, is which, if either, of these models can explain the origin of brachinites.

Petrology of Brachinites

Nehru et al. (1996) have drawn a direct analogy between the formation of the acapulcoite-lodranite clan and the brachinites. One way to evaluate this is through comparison of mineral compositions. The acapulcoite-lodranite clan is a reduced assemblage, while the brachinites are oxidized. Hence, Fe/Mg and Fe/Mn of mafic silicates cannot be used to contrast the origins of these two suites as redox variations and/or subsolidus equilibration may have overprinted variations imposed by mineral-melt equilibria. However, the minor element contents of olivine and pyroxene provide evidence regarding their origins.

The CaO content of olivine in brachinites is distinctly higher than that of acapulcoites, lodranites or equilibrated ordinary chondrites (Fig. 2). In slowly cooled ultramafic rocks, the CaO content of olivine generally decreases as temperature decreases (e.g. see discussion in Smith et al., 1980), although this hasn't been well quantified for low pressure meteoritic compositions. Acapulcoites, lodranites and the L7 chondrite LEW 88663 give empirical evidence for the low CaO contents expected of metamorphic/melting-residue olivines. LEW 88663 and the acapulcoites are rocks heated to high, generally subsolidus temperatures, while the lodranites reached anatectic temperatures (McCoy et al., 1996, 1997; Mittlefehldt and Lindstrom, 2001; Mittlefehldt et al., 1996). The estimated peak temperature range for the acapulcoite-lodranite suite is ~1225-1475°K (McCoy et al., 1996; 1997; Mittlefehldt et al., 1996). In the case of Acapulco, initial cooling from peak temperature was rapid, followed by a period of slower cooling (Pellas et al., 1997). This allowed the mafic silicates to maintain equilibrium to differing temperatures below the peak temperature. Hence, the low CaO contents of acapulcoite-lodranite olivines were established at blocking temperatures well below the solidus.

Brachinite olivine grains have =5 times more CaO than the acapulcoite, lodranite or L7 chondrite olivines (Fig. 2), suggesting an igneous origin (see Smith et al., 1983; Warren and Kallemeyn, 1989). This is supported by comparison with the L chondrite impact-melt PAT 91501. This rock has a clear igneous texture, with euhedral olivines, zoned pyroxenes and interstitial quenched plagioclase and glass (Mittlefehldt and Lindstrom, 2001). The igneous olivines in PAT 91501 have CaO contents that overlap those of the brachinites, and are much higher than those of the L7 chondrite LEW 88663 (Fig. 2).

Ureilite olivines also have high CaO contents, generally higher than those of brachinites (e.g. Goodrich et al., 1987; Singletary and Grove, 2003; Smith et al., 1983). The genesis of ureilites is somewhat controversial, but the consensus is that they are melt residues (see Mittlefehldt et al., 1998). This seems to negate the argument that the high CaO contents of brachinite olivines imply an igneous origin. However, calculations show that ureilite olivine and pigeonite last equilibrated at magmatic temperatures (1473-1573 °K; Singletary and Grove, 2003), and zoning profiles in reduced rims of olivine and pigeonite microtextures show that ureilites were rapidly quenched (2-20 °K hr^{-1}; e.g. Miyamoto et al., 1985; Takeda et al., 1989). The rapid quench from high temperature allowed preservation of high CaO contents in olivine, and thus ureilites do not provide evidence against an igneous origin for brachinites. However, if ureilites are melt residues, then they demonstrate that high CaO contents in olivines do not require crystallization from magma.

Calcium partitioning between olivine and melt is a function of melt Na_2O, Al_2O_3, CaO and FeO contents (Libourel, 1999). The olivines in PAT 91501 crystallized from a melt of L chondrite composition (Mittlefehldt and Lindstrom, 2001). The differences in CaO contents between the most CaO-poor olivines in PAT 91501 and the ALH 84025 or EET 9940n olivines are entirely explicable by the difference in mg# of the olivines (and hence, equilibrium melt). While this might suggest that the parent melt for the brachinites was essentially chondritic in composition, this need not be the case. For given CaO and FeO contents, Al_2O_3 will decrease the Ca partition coefficient while Na_2O will increase it (Libourel, 1999). Hence, a calcium- and aluminum-rich but sodium-poor brachinite parent-melt could crystallize olivines with CaO contents like those of PAT 91501. In addition, the texture of PAT 91501 indicates that it was quenched before it was completely crystallized, while the brachinites have textures of more

slowly cooled igneous rocks. Thus, the blocking temperature for CaO in olivine in PAT 91501 was likely higher.

There is some indication that melts in equilibrium with the brachinites were relatively poor in Na_2O. Clinopyroxenes in the brachinites have much lower Na_2O contents than those of the lodranites (Fig. 3). For lodranite and brachinite clinopyroxenes, the atom ratio (Cr+Al-2*Ti)/Na > 1, indicating that the Na content of the pyroxenes is not limited by availability of charge compensating R^{3+}. The very low Na_2O content of EET 9940n high-Ca pyroxene may partially reflect equilibration with plagioclase, a phase not present in the lodranites shown in Fig. 3. However, ALH 84025 is plagioclase-free (or nearly so), and its pyroxenes are also Na-poor, and acapulcoites contain more sodic plagioclase than EET 9940n (Fig. 4) yet have clinopyroxenes with higher Na_2O contents (Fig. 3). The melt in equilibrium with the brachinites was also Ti-poor compared to that in equilibrium with the lodranites; the TiO_2 contents of the pyroxenes would suggest by about a factor of two (Fig. 3). Comparison of clinopyroxene and spinel compositions of ALH 84025 and EET 9940n show that the latter crystallized from a more aluminous melt (Figs. 3, 5; Tables 2, 3).

The results of our fabric study also suggest an igneous, specifically cumulate, origin for EET 9940n and ALH 84025. This conclusion is based on four general observations: (i) quantitatively confirmed olivine lineations and probable foliations, (ii) the consistency of specific olivine orientation patterns with those of previously measured cumulates, (iii) the relative strength of olivine preferred orientations, and (iv) the absence of internal strain systems produced by solid state flow.

Our petrofabric analysis demonstrates the existence of olivine preferred orientation in EET 99407 and ALH 84025. Particularly in ALH 84025 the patterns reveal a (010) face foliation like that observed by Brothers (1964) in his seminal work on the Rhum and Skaergaard cumulate complexes. In both brachinites the principle lineation is expressed by relatively high [001] (c axis) concentrations, which is at variance with the [100] lineations commonly observed in tectonites (e.g., AveLallemant and Carter, 1970; AveLallemant, 1975; Nicolas et al., 1973). Igneous olivine grains elongated along the c crystallographic axis would be expected to line up in response to convection currents and to preferentially come to rest on their flattened (010) face. The fabric of ALH 84025 fits well with this scenario, but it is less apparent whether that of EET

99407 does. This could arise if the EET 99407 settling environment was more chaotic (turbulent) than that for ALH 84025.

Although our U-stage results show definite olivine preferred orientations, the data also show significant scatter. Many olivine grains conform to recognizable orientation patterns, but many others do not. Figure 13 shows contrast-enhanced photomicrographs of both terrestrial and meteoritic ultramafic rocks, all of which show visible mineral lineations and foliations. Note that tectonites (Fig 13 a,b) show superior orientation fabrics compared to cumulates (Fig. 13 c,d). In addition, general field experience in terrestrial terrains reveals extremely well-developed lineations/foliations in metamorphic rocks compared to more random igneous flow structures. Thus, we suggest that the inherent randomness of antarctic brachinite olivine patterns is more consistent with an igneous origin than a metamorphic/tectonic origin.

Olivine grains in EET 99407 and ALH 84025 do not show any of the microscopic evidence for tectonic strain that is observed in terrestrial tectonites. Specifically, oriented slip planes and kink bands are absent. Undulatory extinction occurs in olivine and pyroxene shows lamellar twinning in both rocks. However, both features are probably shock produced (see Stöffler et al., 1991). Equant olivine grains may form triple junctures but the wide range in boundary angles suggests limited recrystallization, or some degree of grain enlargement by reaction with silicate pore fluids. Plagioclase in EET 9940n and high-Ca pyroxene in both brachinites partially to completely enclose olivine grains, a common igneous texture. In sum, brachinite olivine grains in our study show no fabric evidence for compaction- or tectonically-induced strain, nor do they show evidence for significant recrystallization. Fabrics and overall textures point to an igneous origin, probably as cumulates.

Although we argue that the textures of the brachinites are inconsistent with metamorphic recrystallization, there is evidence that EET 9940n was annealed after shock. We estimated an S3 shock stage from the undulatory extinction and planar fractures in olivine grains. The dusty appearance caused by abundant μm-sized inclusions of troilite and rare metal in all phases in EET 9940n (Fig. 1) is like that of shock-darkened ordinary chondrites (Rubin, 1992; Stöffler et al., 1991), and is consistent with an S3 shock stage. The plagioclase patches, however, are composed of numerous μm-sized grains, and contain vesicles. This is not expected for shocked or unshocked, cumulus or residual plagioclase grains. Mikouchi et al. (2002) report preliminary

work on reheating maskelynite at 900°C for 24 hours. In these experiments, the maskelynite crystallized to numerous grains with a fibrous texture, and rounded vesicles ~100 μm in size were formed. There is an overall similarity of this texture to that observed in EET 9940n, although the fine-grained plagioclase in the latter is not fibrous. This suggests that the plagioclase patches in the latter could represent devitrified maskelynite. Maskelynite formation implies a shock stage of S5, which suggests that strong mosaicism should be present in olivine (Stöffler et al., 1991). It seems unlikely that the mild heating needed to devitrify maskelynite would entirely anneal-out evidence for mosaicism in olivine. Nevertheless, mild post-shock metamorphism is indicated by the plagioclase textures.

Geochemistry of Brachinites

The few brachinites studied show a wide range in incompatible lithophile element abundances (Fig. 8). Brachina has essentially chondritic rare earth element (REE) abundances (Nehru et al., 1983), and is very similar to acapulcoites such as ALHA81261 (Fig. 8). ALH 84025 shows moderate depletions in REE^{3+}, with an excess in Eu (Warren and Kallemeyn, 1989). Warren and Kallemeyn (1989) inferred that minor plagioclase must have been present in their sample to explain the high Eu/Sm ratio, in spite of its absence in all thin sections (Table 1). This is supported by ion microprobe analyses of REE in olivine, augite and Ca-phosphate in ALH 84025, none of which had anomalous Eu contents (Wadhwa et al., 1998b). Thus, a Eu-rich phase, most plausibly plagioclase, must have been present in the sample analyzed by Warren and Kallemeyn (1989). EET 9940n exhibits an extreme depletion in REE^{3+}, with a large excess in Eu. These latter brachinites have very different REE patterns from basalt-depleted lodranites such as MAC 88177 (Fig. 8). The pattern for EET 9940n in particular is similar to igneous rocks bearing cumulus plagioclase.

Nehru et al. (1983; 1996) have suggested that brachinites were formed by metamorphism of chondritic material with some being anatectic residues, analogous to the acapulcoite-lodranite clan. Goodrich (1998) modeled the major element compositions of ALH 84025, Brachina and Eagles Nest, and concluded that these meteorites could represent a suite of anatectic residues, but only if the parent body was originally heterogeneous with respect to refractory lithophile elements. With the addition of new data on EET 9940n, the mineralogy and incompatible lithophile element contents of brachinites show that this model is untenable. Melting of sodic

plagioclase-peridotites (that is, something akin to ordinary chondrites) will result in exhaustion of plagioclase from the source before augite (Stolper et al., 1979). Hence, residues with lower plagioclase contents should have lower REE contents than more plagioclase-rich residues. This is opposite what is shown in Fig. 8 assuming both ALH 84025 and EET 9940n are residues. EET 9940n contains 4-5% plagioclase, and the Eu excess indicates that at least a portion of this plagioclase would have to be residual, rather than quenched from a trapped melt. ALH 84025 has a lower plagioclase content as indicated by thin section modes and the lower bulk rock Eu content compared to EET 9940n (Table 1; Fig. 8). The higher REE content of ALH 84025 cannot be explained-away by arguing that it contains a trapped melt component, elevating its incompatible element content, because the trapped melt would have crystallized plagioclase. Using mineral/melt partition coefficients for olivine, augite and plagioclase calculated after Jones (1995) and the pseudo-normative mineralogy for EET 9940n calculated above, a melt in equilibrium with it would have ~60× the Sm as measured for EET 9940n. Assuming this is the composition of a possible trapped melt, then ~5% trapped melt would be required to explain the measured Sm content of ALH 84025. The trapped melt may have been ultramafic (see below) with roughly 25% normative plagioclase. Failure to observe ~1% plagioclase in any thin section of ALH 84025 (see Warren and Kallemeyn, 1989) can only be explained by claiming that only the bulk sample analyzed contained the trapped melt component. The same calculation would suggest that ALH 84025 should have roughly twice the Eu measured, making even this latter case impossible. Because ALH 84025 has a superchondritic Eu/Sm ratio, any plagioclase present in the bulk sample could not simply represent quenched trapped melt – it must represent plagioclase fractionated from a melt. This further exacerbates the problems for a melt-residue model. For these reasons, it is unlikely that ALH 84025 and EET 9940n are part of a suite of anatectic residues from a primitive source similar to Brachina in lithophile element composition.

The alternative model is that brachinites represent cumulates. The high Eu/Sm ratio for EET 9940n indicates that at least some of the plagioclase equilibrated with a melt, and is therefore cumulus. Plagioclase patches are generally irregular in shape, partially enclose olivine and augite grains, and are interstitial – not a texture expected for grains that accumulated from a magma. This suggests either that the plagioclase formed by heteradcumulus growth from the magma, or (less likely) that a subsequent shock and devitrification obscured the original texture. The moderately high Eu/Sm ratio for ALH 84025 is also consistent with cumulus plagioclase.

As was the case for the anatectic residue model, the higher REE content of ALH 84025 compared to EET 9940n does not support a simple crystallization sequence from a common parent magma for these brachinites. The crystallization sequence would most likely be olivine → olivine+augite → olivine+augite+plagioclase (Stolper et al., 1979). Thus, EET 9940n, with higher plagioclase contents, should also have higher REE contents, contrary to measurement. Thus distinct parent magmas are indicated.

Above we calculated that a parent melt in equilibrium with EET 9940n would have a Sm content ~60× that of the cumulate, or roughly ~3× CI chondrites. Assuming a parent body with approximately CI abundances of refractory lithophile elements, the parent melt of EET 9940n would then represent about 30% melting of its source region. Melting experiments on ordinary chondrite compositions show that plagioclase and high-Ca pyroxene will be exhausted from the source regions at about 15% melting (Jurewicz et al., 1995). Melts become increasingly ultramafic as the degree of melting increases. Thus, the low Sm content of EET 9940n argues for an ultramafic, rather than a basaltic, parent melt.

The siderophile element-Se pattern of brachinites is compared to that of acapulcoite-lodranite clan meteorites in Fig. 9. Mittlefehldt et al. (1996) presented an interpretation of the siderophile element and Se contents in acapulcoite-lodranite clan meteorites. ALHA81261 is a typical acapulcoite in that its composition reflects nebular processes (condensation and accretion), not parent body processes (melting and melt migration). It shows an unfractionated siderophile element pattern, with a depletion of Se relative to CI chondrites due to depletion of moderately volatile elements in the acapulcoite-lodranite parent body. EET 84302 is transitional - its lithophile element abundances are nebular, while the siderophile element and Se contents reflect the loss of a partial melt in the metal-sulfide system. Bulk samples of EET 84302 have high Ir/Ni ratios, but very low Se/Co ratios – broadly consistent with metal remaining after loss of a metal-sulfide partial melt. The very low Se content of EET 84302 could partially reflect heterogeneous distribution of troilite in this coarse-grained achondrite (see Takeda et al., 1994). FRO 90011 is a partial melt residue. It has a lithophile element signature demonstrating loss of a basaltic partial melt, and a siderophile element-Se signature indicating loss of a metal-sulfide partial melt. Finally, MAC 88177 represents an unusual combination of processes. The lithophile element signature shows that a basaltic partial melt was lost from this lodranite, but the siderophile element-Se signature is that of a metal-sulfide partial melt. This suggests that a

portion of the metal and sulfide present in MAC 88177 was formed from a metal-sulfide melt that invaded and crystallized in a basalt-depleted rock.

The siderophile element-Se patterns of the brachinites are distinct from any of the acapulcoite-lodranite clan meteorites. All brachinites show an enrichment in Co relative to other siderophile elements. The brachinites are relatively oxidized assemblages – the olivines have moderately high FeO contents and FeO/MnO ratios (Tables 1, 2), the metal and sulfide are Ni-rich (Table 4), and the NiO content of olivine, while low, is higher than observed in Lodran (see Papike et al., 1995). The few brachinites studied in detail show evidence for oxidation or reduction having affected the suite. There is a general increase in olivine FeO/MnO that is correlated with FeO/MgO (Fig. 14). Igneous processes will substantially fractionate FeO/MgO, but not FeO/MnO (e.g. Mittlefehldt, 1986). The correlation shown is consistent with Fe/FeO redox reactions. Similarly, there is a correlation between high-Ca pyroxene wollastonite content and FeO/MnO (Fig. 14) that is also consistent with redox reactions. In the absence of low-Ca pyroxene, the wollastonite content of high-Ca pyroxene will decrease as bulk rock FeO decreases, other things being equal. This is because the total cation/Si ratio decreases, decreasing the normative olivine/pyroxene ratio of the rock, forcing the available Ca to be contained in an increasing amount of pyroxene. (Trace orthopyroxene is present in Brachina, but only in quenched melt inclusions in olivine (Nehru et al., 1983). It is unlikely the composition of augite reflects equilibration with this orthopyroxene.)

Cobalt is the most easily oxidizable of the four siderophile elements shown in Fig. 9, and the enhanced Co content of brachinites relative to other siderophile elements likely reflects substantial lithophile character for it. There is a fairly good correlation of bulk rock Co/Ir with olivine FeO/MnO (Fig. 14), consistent with partial oxidation of Co in brachinites. However, this evidence should be evaluated cautiously because igneous processes can fractionate Ir from Co (e.g. Scott, 1972). Nickel has a liquid metal/solid metal partition coefficient only slightly less than that of Co (Jones and Malvin, 1990), and Co/Ni ratios will be much less affected by igneous processes. The Co/Ni ratio for EET 9940n is much higher than those of the other brachinites, which are roughly equal and not correlated with olivine FeO/MnO (Fig. 14). Gold is the most incompatible of the four siderophile elements shown in Fig. 9. EET 9940n has the lowest Au/Ir coupled with the highest Co/Ir (Fig. 14), which is inconsistent with simple igneous fractionation

in the metal-sulfide system. Thus, there is good evidence that the high Co/Ir of EET 9940n is primarily due to partial lithophile character for Co.

The case is less clear for the other three brachinites. The increasing Co/Ir with Au/Ir is broadly consistent with igneous fractionation in the metallic system, and it is difficult to separate igneous from possible redox effects. ALH 84205, with the highest Au/Ir ratio, is the most fractionated of the remaining three brachinites, and should have a lower Co/Ni ratio than the others based on experimental partition coefficients (Jones and Malvin, 1990). ALH 84025 has the highest FeO/MnO of the three (Fig. 14), and oxidation would raise the Co/Ni of a rock crystallized from an oxidized magma. Thus, a combination of siderophile element igneous fractionation and oxidation could combine to obscure clear trends of bulk rock Co/Ir with olivine FeO/MnO.

Mineral FeO/MnO ratios provide strong evidence for differences in oxidation among brachinites, and variations in Co/Ir are consistent with this. Because bulk rock siderophile element ratios show evidence for redox variations, this process must have occurred during or prior to crystallization of the brachinite parent magmas - in situ redox of solidified cumulates would not alter bulk rock Co/Ir. One possibility is that brachinite parent melts were formed from different source regions with differing degrees of oxidation. In this case, FeO/MnO and Co/Ir may have been passed through the magma stage with little change. The alternate case is that the magma contained a redox agent that acted variably on the melt, producing the range in observed geochemical characteristics. At present, we cannot definitively demonstrate which may be correct because there is no direct evidence as to the nature of the redox agent responsible.

Petrogenesis of Brachina

Brachina has a relatively unfractionated refractory lithophile element pattern (e.g. Mittlefehldt, 2003; Nehru et al., 1983; see Fig. 8), which limits formation models to those that do not cause fractionation of incompatible lithophile elements – metamorphism of chondritic material (Nehru et al., 1983), formation of a chondritic composition melt (Johnson et al., 1977), possibly by impact (Ryder, 1982), or as an orthocumulate in which the melt component determines the incompatible element contents (Warren and Kallemeyn, 1989). The siderophile and chalcophile element abundances further constrain permissible models.

Nehru et al. (1983) explained the siderophile-chalcophile element pattern of Brachina as reflecting the loss of a (Fe,Ni)S melt, a model invoked for some members of the acapulcoite-lodranite clan (Mittlefehldt et al., 1996). Brachina shows a siderophile-chalcophile element pattern distinct from those of the latter meteorites (Fig. 9). In particular, Brachina has superchondritic Se/Ni and Se/Au ratios while acapulcoites and lodranites that have lost a partial melt in the Fe-Ni-S system have subchondritic ratios (EET 84302 and FRO 90011 in Fig. 9). Thus, it is unlikely that Brachina was formed by high-temperature metamorphism and metal-sulfide melting of chondritic material à la Nehru et al. (1983).

Johnson et al. (1977) posited that Brachina represented a chondritic composition melt. The siderophile-chalcophile element depletion observed indicates that this cannot be correct in detail, but without a suggested mechanism, the model cannot be evaluated.

Comparison of the siderophile-chalcophile element pattern and texture of PAT 91501, an impact-melt of L chondrite material, with Brachina allows evaluation of impact melting as a formation mechanism. The patterns for PAT 91501 and Brachina are generally similar, though PAT 91501 has a lower Ir/Co ratio (0.21 vs. 0.60 for Brachina; Fig. 9), and is more depleted in all elements shown. The silicate texture shows that PAT 91501 cooled much faster that Brachina – the former contains zoned pyroxene and chromite grains, quench-textured plagioclase grains, and interstitial Si-Al-alkali-rich glass (Mittlefehldt and Lindstrom, 2001) while Brachina has a generally equilibrated texture (Nehru et al., 1983). In spite of the rapid cooling implied by the texture, immiscible metal-sulfide melts were more efficiently separated from silicate melt in PAT 91501. Shearing forces acting on the impact-melt may facilitate this separation. Norman and Mittlefehldt (2002) noted that coarse metal nodules were concentrated along the axis of a large intrusive impact-melt dike in the Chico L6 chondrite, which they suggested indicated flow differentiation. Thus, comparison of textures and siderophile-chalcophile element depletions in PAT 91501 and Brachina indicate that an impact-melt origin for the latter is unlikely.

Warren and Kallemeyn (1989) suggested that Brachina represents an orthocumulate, and this is consistent with the lithophile element abundances. This requires that the incompatible lithophile element pattern is dominated by the melt phase, and in the combined proportions, the cumulus and melt components have approximately chondritic abundances of the lithophile elements. It is less certain whether this model can explain the siderophile element abundances.

Cumulate eucrites are the only asteroidal cumulates available for comparison. These have much lower siderophile element abundances, for example the Ir contents of cumulate eucrites are ~3×10^{-5} to 2×10^{-3} that of Brachina (e.g. see Mittlefehldt et al., 1998). However, basaltic eucrites, plausible parent melt compositions for cumulate eucrites, have very low siderophile element contents that seem to require an earlier, efficient separation of metal from silicate (see discussions in Mittlefehldt and Lindstrom, 2003; Righter and Drake 1996; 1997). Thus, cumulate eucrites may not be a good model for Brachina. Cobalt and Ni partitioning between metal, metallic melt and silicate melt depend on oxygen fugacity, S content, temperature and silicate melt composition (Righter and Drake, 1996), which are not well known for the brachinite parent body. Brachinites were formed at higher oxygen fugacity and from a more ultramafic melt than eucrites, which would permit higher Co and Ni contents in silicate melts. However, they were also formed from higher temperature melts and the parent body likely had a higher S content than the eucrite parent body, which would act to lower the Co and Ni contents of brachinite parent melts. Siderophile-chalcophile element abundances cannot presently be used to quantitatively evaluate an orthocumulate model for Brachina.

Chronology of Brachinites

Several lines of evidence indicate that the brachinites formed early in solar system history but experienced later heating. In addition to the presence in Brachina, ALH 84025, and Eagles Nest of excess ^{129}Xe (Ott et al., 1987; Swindle et al., 1998; this study), Crozaz and Pellas (1984) reported high particle track densities attributed to fission of extinct ($t_{½}$ 82 Ma) ^{244}Pu in Brachina, and Wadhwa et al. (1998a) found excess ^{53}Cr from the decay of extinct ($t_{½}$ 3.7 Ma) ^{53}Mn in it. A whole rock sample of Brachina gave a ^{147}Sm/^{143}Nd model age, relative to the eucrite initial, of 4.61 Ga. On the other hand, the ^{87}Rb-^{87}Sr chronometer in Brachina is disturbed, and the data suggest an apparent age of 2.5 Ga (Bogard et al., 1983).

The Ar-Ar ages of EET 99402, Brachina, and probably Eagles Nest indicate significant late degassing of radiogenic ^{40}Ar. Our results for Brachina and EET 99402 show evidence for degassing at 4.13 Ga, and this may indicate a common degassing event for them. Given the relatively young age, a large impact on the asteroid parent body seems the most likely heating mechanism. Our petrographic observations on EET 9940n show that the plagioclase may have been shock-modified to maskelynite, which subsequently devitrified. While it is tempting to

equate this petrographic evidence with the event that outgassed radiogenic Ar, we caution that olivine textures of EET 99402 indicate lower shock-loading, and that Nehru et al. (1983) found no evidence for shock in Brachina. The disturbance of the Ar-Ar chronometer in EET 99402 and Brachina, the Rb-Sr chronometer in Brachina, and the I-Xe chronometer in Eagles Nest may have been produced by a single impact heating event on the brachinite parent body. But if so, it left differing petrographic imprints on the samples.

CONCLUSIONS

EET 99402 and EET 99407 are paired brachinites based on texture, mineralogy, mineral composition and bulk composition. EET 9940n is highly depleted in incompatible lithophile elements, except for Eu, and in siderophile elements, except for Co. The texture is igneous, with high-Ca pyroxene and plagioclase occurring in part as interstitial grains partially to completely enclosing olivine grains, and with some large irregular olivine grains having deeply embayed margins. Similar textures are described for ALH 84025 and Eagles Nest (Swindle et al., 1998; Warren and Kallemeyn, 1989). Petrofabric analysis demonstrates that olivine grains in ALH 84025 and EET 9940n show distinct lineations and probable foliations. The textures support an igneous cumulate origin for these brachinites.

Minor element contents of olivine and pyroxene in ALH 84025 and EET 9940n have distinctly different characteristics than those of the acapulcoite-lodranite clan – a suite of high-grade metamorphic rocks to anatectic residues. The high CaO contents of olivines indicate a higher temperature of equilibration for the brachinites, consistent with an igneous origin. Brachinite olivines have CaO contents like those of olivines from PAT 91501, an impact-melt of L chondrite material, and much higher than those of olivine in the L7 chondrite LEW 88663, further supporting an igneous origin for brachinites. Ureilites, believe to be melt-residues, also have high CaO contents in their olivines (e.g. Smith et al., 1983), indicating that olivine compositions may not uniquely define mode of origin.

The brachinite suite shows a broad correlation between olivine FeO/MnO and bulk rock Co/Ir suggesting that the suite was formed at slightly varying redox conditions. At present, it is not clear whether the source regions of the parent magmas were at differing redox state, or whether redox processes occurred in the magmas during crystallization.

Brachina contains excess ^{129}Xe correlated with reactor-produced ^{128}Xe indicating that short-lived ^{129}I was present at the time of formation. This is consistent with fission-particle track excesses from ^{244}Pu, Cr isotopic data, and other Xe isotopic studies showing that brachinites were formed early in solar system history (Crozaz and Pellas, 1984; Ott et al., 1987; Swindle et al., 1998; Wadhwa et al., 1998a). The Ar-Ar age spectra of both Brachina and EET 99402 show evidence for later reheating at about 4.13 Ga ago, possibly indicating a common impact event. However, Brachina is unshocked (Nehru et al., 1983), while EET 9940n shows textural evidence that its plagioclase may have been shocked to maskelynite and subsequently devitrified. Hence, there is no clear link between texture and Ar-Ar ages that can be unambiguously interpreted.

Studies of recently found brachinites have shown that their petrologic and geochemical characteristics indicate igneous origins (Swindle et al., 1998; Warren and Kallemeyn, 1989; this work). Brachina is described as having an igneous texture (Floran et al., 1978; Nehru et al., 1983) and its olivines have high CaO contents indicating a high temperature origin (Smith et al., 1983). We infer that all brachinites are igneous rocks derived from a differentiated parent asteroid. Their parent melts were ultramafic in composition, indicating high degrees of melting of the source regions. There is too little information on too few brachinites at this point to develop detailed models regarding the petrologic evolution of the brachinite parent asteroid.

Acknowledgments—We thank John Schutt for "locating" the EET 99402 and EET 99407 samples so that the robot NOMAD could "find" them. We thank M.T. Lee and C. Galindo Jr. for technical support with some of the electron microbeam work. We thank C.S. Schwandt for doing the x-ray mapping of thin sections and calculation of modes. We thank the National Science Foundation for funding the ANSMET and NOMAD collecting teams that brought back ALH 84025, EET 99402 and EET 99407, and the Meteorite Working Group, NASA-Johnson Space Center and the National Museum of Natural History (Smithsonian Institution) for allocation of the samples. We thank the late M. Prinz and the American Museum of Natural History for supplying the sample of Brachina. Reviews by C. Floss and C.A. Goodrich, and editorial handling by E.R.D. Scott led to substantial improvements – they are thanked. The Cosmochemistry Program through NASA RTOPs #344-31-30-01 to D.D. Bogard and #344-31-10-18 to D.W. Mittlefehldt supported this work.

REFERENCES

AveLallemant H. G. (1975) Mechanisms of preferred orientations of olivine in tectonite peridotites. *Geology* **3**, 653-656.

AveLallemant H. G. and Carter N. L. (1970) Syntectonic recrystallization of olivine and modes of flow in the upper mantle. *Bull. Geol. Soc. Amer.* **81**, 2203-2220.

Berkley J. L., Brown H. G., Keil K., Carter N. L., Mercier J-C. C. and Huss, G. (1976) The Kenna ureilite: An ultramafic rocks with evidence for igneous, metamorphic, and shock origin. *Geochim. Comochim. Acta* **40**, 1429-1437.

Bogard D.D. and Garrison D.H. (2003) ^{39}Ar-^{40}Ar ages of eucrites and the thermal history of asteroid 4-Vesta. *Meteoritics Planet. Sci.*, in press.

Bogard D.D., Nyquist L.E., Johnson P., Wooden J. and Bansal B. (1983) Chronology of Brachina (abstract). *Meteoritics* **18,** 269-270.

Bogard D.D., Garrison D.H., Norman M., Scott E.R.D., and Keil K. (1995) ^{39}Ar-^{40}Ar age and petrology of Chico: Large-scale impact melting on the L chondrite parent body. *Geochim. Comochim. Acta* **59**, 1383-1399.

Brearley A.J. and Jones R.H. (1998) Chondritic meteorites. In *Planetary Materials* (ed. J.J. Papike), pp. 3-1 to 3-398. Reviews in Mineralogy, **36,** Min. Soc. Am., Washington, D.C., USA.

Brothers R. N. (1964) Petrofabric analysis of Rhum and Skaergaard layered rocks. *J. Petrol.* **5**, 255-274.

Crozaz G. and Pellas P. (1984) The formation age of the Brachina meteorite. *Earth Planet. Sci. Lett.* **71,** 195-199.

Floran R.J., Prinz M., Hlava P.F., Keil K., Nehru C.E. and Hinthorne J.R. (1978) The Chassigny meteorite: a cumulate dunite with hydrous amphibole-bearing melt inclusions. *Geochim. Cosmochim. Acta* **42,** 1213-1229.

Garrison D., Hamlin S., and Bogard D. (2000) Chlorine abundances in meteorites. *Meteoritics Planet. Sci.* **35**, 419-429.

Goodrich C.A. (1998) Brachinites: Residues from low degrees of melting of a heterogeneous parent body (abstract). *Meteoritics Planet. Sci.* **33,** A60.

Goodrich C.A., Jones J.H. and Berkley J.L. (1987) Origin and evolution of the ureilite parent magmas: Multi-stage igneous activity on a large parent body. *Geochim. Cosmochim. Acta* **51,** 2255-2273.

Grady M.M. (2000) *Catalogue of Meteorites*, 5th ed. Cambridge Univ. Press, Cambridge, UK.

Johnson J.E., Scrymgour J.M., Jarosewich E. and Mason B. (1977) Brachina meteorite - a chassignite from South Australia. *Rec. S. Australia Mus.* **17,** 309-319.

Jones J.H. (1995) Experimental trace element partitioning. In *Rock Physics and Phase Relations. A Handbook of Physical Constants*, 73-104.

Jones J.H. and Malvin D.J. (1990) A nonmetal interaction model for the segregation of trace metals during solidification of Fe-Ni-S, Fe-Ni-P, and Fe-Ni-S-P alloys. *Metall. Trans.* **21B,** 697-706.

Jurewicz A.J.G., Mittlefehldt D.W. and Jones J.H. (1995) Experimental partial melting of the St. Severin (LL) and Lost City (H) chondrites. *Geochim. Cosmochim. Acta* **59,** 391-408.

Libourel G. (1999) Systematics of calcium partitioning between olivine and silicate melt: implications for melt structure and calcium content of magmatic olivines. *Contrib. Mineral. Petrol.* **136,** 63-80.

Mason B., MacPherson G.J., Score R., Martinez R., Satterwhite C., Schwarz C. and Gooding J.L. (1992) Descriptions of stony meteorites. *Smith. Contrib. Earth Sci.* **30,** 17-35.

McCoy T.J., Keil K., Clayton R.N., Mayeda T.K., Bogard D.D., Garrison D.H., Huss G.R., Hutcheon I.D. and Wieler R. (1996) A petrologic, chemical, and isotopic study of Monument Draw and comparison with other acapulcoites: Evidence for formation by incipient partial melting. *Geochim. Cosmochim. Acta* **60,** 2681-2708.

McCoy T.J., Keil K., Clayton R.N., Mayeda T.K., Bogard D.D., Garrison D.H. and Wieler R. (1997) A petrologic and isotopic study of lodranites: Evidence for early formation as partial melt residues from heterogeneous precursors. *Geochim. Cosmochim. Acta* **61,** 623-637.

Mercier J-C. C. and Nicolas A. (1975) Textures and fabrics of upper-mantle peridotites as illustrated by xenoliths from basalts. *J. Petrol.* **16**, 454-487.

Mikouchi T., Miyamoto M., Koizumi E., Monkawa A. and McKay G. (2002) Maskelynite recrystallization: Implications for shock and reheating histories of several achondrites (abstract). *Meteoritics Planet. Sci.* **37,** A100.

Mittlefehldt D.W. (1986) Fe-Mg-Mn relations of ureilite olivines and pyroxenes and the genesis of ureilites. *Geochim. Cosmochim. Acta* **50,** 107-110.

Mittlefehldt D.W. (1994) The genesis of diogenites and HED parent body petrogenesis. *Geochim. Cosmochim. Acta* **58,** 1537-1552.

Mittlefehldt D.W. (2003) 1.09 Achondrites. In *Treatise on Geochemistry, Volume 1: Meteorites, Comets, and Planets* (ed. A.M. Davis). Elsevier, in press.

Mittlefehldt D.W. and Berkley J.L. (2002) Petrology and geochemistry of paired brachinites EET 99402 and EET 99407 (abstract). *Lunar Planet. Sci. XXXIII*, 1008.

Mittlefehldt D.W. and Lindstrom M.M. (2001) Petrology and geochemistry of Patuxent Range 91501, a clast-poor impact-melt from the L chondrite parent body, and Lewis Cliff 88663, an L7 chondrite. *Meteoritics Planet. Sci.* **36,** 439-457.

Mittlefehldt D.W. and Lindstrom M.M. (2003) Geochemistry of eucrites: Genesis of basaltic eucrites, and Hf and Ta as petrogenetic indicators for altered antarctic eucrites. *Geochim. Cosmochim. Acta* **67,** 1911-1935.

Mittlefehldt D.W., Lindstrom M.M., Bogard D.D., Garrison D.H. and Field S.W. (1996) Acapulco- and Lodran-like achondrites: Petrology, geochemistry, chronology and origin. *Geochim. Cosmochim. Acta* **60,** 867-882.

Mittlefehldt D.W., McCoy T.J., Goodrich C.A. and Kracher A. (1998) Non-chondritic meteorites from asteroidal bodies. In *Planetary Materials* (ed. J.J. Papike), pp. 4-1 to 4-195. Reviews in Mineralogy, **36,** Min. Soc. Am., Washington, D.C., USA.

Miyamoto M., Takeda H. and Toyoda H. (1985) Cooling history of some antarctic ureilites. *Proc. 16th Lunar Planet. Sci. Conf., J. Geophys. Res.* **90,** (Suppl.), D116-D122.

Nehru C.E., Prinz M., Delaney J.S., Dreibus G., Palme H., Spettel B. and Wänke H. (1983) Brachina: A new type of meteorite, not a Chassignite. *Proc. 14th Lunar Planet. Sci. Conf., J. Geophys. Res.* **88,** (Suppl.), B237-B244.

Nehru C.E., Prinz M., Weisberg M.K., Ebihara M.E., Clayton R.N. and Mayeda T.K. (1992) Brachinites: A new primitive achondrite group (abstract). *Meteoritics* **27,** 267.

Nehru C.E., Prinz M., Weisberg M.K., Ebihara M.E., Clayton R.N. and Mayeda T.K. (1996) A new brachinite and petrogenesis of the group (abstract). *Lunar Planet. Sci. XXVII*, 943-944.

Nicolas A., Boudier F. and Boullier A.M. (1973) Mechanisms of flow in naturally and experimentally deformed peridotites. *Am. J. Sci.* **273,** 853-876.

Norman M.D. and Mittlefehldt D.W. (2002) Impact processing of chondritic planetesimals: Siderophile and volatile element fractionation in the Chico L chondrite. *Meteoritics Planet. Sci.* **37,** 329-344.

Ott U., Löhr H.P. and Begemann F. (1985) Noble gases and the classification of Brachina. *Meteoritics* **20,** 69-78.

Ott U., Begemann F. and Löhr H.P. (1987) Noble gases in ALH 84025: Like Brachina, unlike Chassigny (abstract). *Meteoritics* **22,** 476-477.

Papike J.J., Spilde M.N., Fowler G.W., Layne G.D. and Shearer C.K. (1995) The Lodran primitive achondrite: Petrogenetic insights from electron and ion microprobe analysis of olivine and orthopyroxene. *Geochim. Cosmochim. Acta* **59,** 3061-3070.

Pellas P., Fiéni C., Trieloff M. and Jessberger E.K. (1997) The cooling history of the Acapulco meteorite as recorded by the ^{244}Pu and ^{40}Ar-^{39}Ar chronometers. *Geochim. Cosmochim. Acta* **61,** 3477-3501.

Righter K. and Drake M.J. (1996) Core formation in Earth's Moon, Mars, and Vesta. *Icarus* **124,** 513-529.

Righter K. and Drake M.J. (1997) A magma ocean on Vesta: Core formation and petrogenesis of eucrites and diogenites. *Meteoritics Planet. Sci.* **32,** 929-944.

Rubin A.E. (1992) A shock-metamorphic model for silicate darkening and compositionally variable plagioclase in CK and ordinary chondrites. *Geochim. Cosmochim. Acta* **56,** 1705-1714.

Rubin A.E., Kallemeyn G.W. and Wasson J.T. (2002) A IAB-complex iron meteorite containing low-Ca clinopyroxene: Northwest Africa 468 and its relationship to lodranites and formation by impact melting. *Geochim. Cosmochim. Acta* **66,** 3657-3671.

Russell S.S., Zipfel J., Grossman J.N. and Grady M.M. (2002) The Meteoritical Bulletin, No. 86, 2002 July. *Meteoritics Planet. Sci.* **37,** A157-A184.

Ryder G. (1982) Siderophiles in the Brachina meteorite: impact melting? *Nature* **299,** 805-807.

Scott E.R.D. (1972) Chemical fractionation in iron meteorites and its interpretation. *Geochim. Cosmochim. Acta* **36,** 1205-1236.

Singletary S.J. and Grove T.L. (2003) Early petrologic processes on the ureilite parent body. *Meteoritics Planet. Sci.* **38,** 95-108.

Smith J.V., Hansen E.C. and Steele I.M. (1980) Lunar highland rocks: Element partitioning among minerals II: Electron microprobe analyses of Al, P, Ca, Ti, Cr, Mn and Fe in olivine. *Proc. Lunar Planet. Sci. Conf. 11th*, 555-569.

Smith J.V., Steele I.M. and Leitch C.A. (1983) Mineral chemistry of the shergottites, nakhlites, Chassigny, Brachina, pallasites and ureilites. *Proc. 14th Lunar Planet. Sci. Conf., J. Geophys. Res.,* **88,** (Suppl.), B229-B236.

Swindle T.D., Kring D.A., Burkland M.K., Hill D.H. and Boynton W.V. (1998) Noble gases, bulk chemistry, and petrography of olivine-rich achondrites Eagles Nest and Lewis Cliff 88763: Comparison to brachinites. *Meteoritics Planet. Sci.* **33,** 31-48.

Stöffler D., Keil K. and Scott E.R.D. (1991) Shock metamorphism of ordinary chondrites. *Geochim. Cosmochim. Acta* **55,** 3845-3867.

Stolper E., McSween H.Y. Jr. and Hays J.F. (1979) A petrogenetic model of the relationships among achondritic meteorites. *Geochim. Cosmochim. Acta* **43,** 589-602.

Takeda H., Mori H. and Ogata H. (1989) Mineralogy of augite-bearing ureilites and the origin of their chemical trends. *Meteoritics* **24,** 73-81.

Takeda H., Mori H., Hiroi T. and Saito J. (1994) Mineralogy of new Antarctic achondrites with affinity to Lodran and a model of their evolution in an asteroid. *Meteoritics* **29,** 830-842.

Wadhwa M., Shukolyukov A. and Lugmair G.W. (1998a) ^{53}Mn-^{53}Cr systematics in Brachina: A record of one of the earliest phases of igneous activity on an asteroid (abstract). *Lunar Planet. Sci. XXIX,* 1480.

Wadhwa M., Zipfel J. and Davis A.M. (1998b) Constraints on the formation history of brachinites from rare-earth-element distributions (abstract). *Meteoritics Planet. Sci.* **33,** A161.

Warren P.H. and Kallemeyn G.W. (1989) Allan Hills 84025: The second Brachinite, far more differentiated than Brachina, and an ultramafic achondritic clast from L chondrite Yamato 75097. *Proc. 19th Lunar Planet. Sci. Conf.,* 475-486.

Weigel A., Eugster O., Koeberl C., Michel R., Krähenbühl U. and Neumann S. (1999) Relationships among lodranites and acapulcoites: Noble gas isotopic abundances, chemical composition, cosmic-ray exposure ages, and solar cosmic ray effects. *Geochim. Cosmochim. Acta* **63,** 175-192.

Wlotzka F. (1993) A weathering scale for the ordinary chondrites (abstract). *Meteoritics* **28,** 460.

Zipfel J. and Palme H. (1993) Chemical composition of new acapulcoites and lodranites (abstract). *Lunar Planet. Sci.* **XXIV,** 1579-1580.

Table 1. Petrologic synopsis of brachinites.

meteorite	pairing	mode (vol %)								olivine		opx		cpx		plag	cm	ref
		oliv	cpx	opx	plag	crm	phos	sulf	met	mg#	Fe/Mn	wo	mg#	wo	mg#	an	mg#	
ALH 84025		79-90	4-15	none	none	0.8-2	tr	3-4	<1%	68	69	-	-	43	81	-	18	1,2
ALH 84025,6*		83.3	9.4	none	none	0.84	0.16	5.4	0.96									2
ALH 84025,26*		86.9	6.4	none	none	0.57	tr	5.4	0.66									2
Brachina		80.4	5.5	tr	9.9	0.5	0.5	3.2	tr	69	68	4	73	39	79	22	30	3,4
Eagles Nest		81	6	none	none	<2	tr	7	yes	68	61	-	-	45	82	-	18	5
EET 99402		87.2	4.6	none	6.3	0.9	-	1.0	tr	64	77	-	-	46	81	-	22	2
EET 99402,22*		86.0	5.0	none	8.1	0.79	tr	0.11	none									2
EET 99407	EET 99402	85.2	4.1	none	9.1	0.6	-	1.0	tr	64	77	-	-	46	81	40	22	2
Hughes 026		92.7	3.6	1.6	<0.1	0.8	0.1	1.2	<0.1	65	-	3	71	47	81	32	20	6
NWA 595		80	5-10	10-15	none	minor	-	tr	-	71	52	2	74	45	82	-	25	7
Nova 003	Reid 013?	yes	yes	yes	yes	-	-	-	-	68	-	2	73	45	80	33	-	8
Reid 013		yes	yes	yes	yes	-	-	-	-	66	-	2	72	46	80	32	-	8
Reid 027		yes	yes	yes	abund	yes	yes	yes	yes	64-66	-	2-3	71-73	38-45	84	14	9	8

References: 1 - Warren and Kallemeyn (1989); 2 - this work; 3 - Nehru et al. (1983); 4 - Smith et al. (1983); 5 - Swindle et al. (1998); 6 - Nehru et al. (1996); 7 - Russell et al. (2002); 8 - Grady (2000)

*Modes determined from elemental mapping of thin sections; see text.

Table 2. Average compositions for representative olivine, high-Ca pyroxene and plagioclase grains from ALH 84025, EET 99402 and EET 99407.

	olivine										high-Ca pyroxene								plagioclase	
	ALH 84025				EET 99402				EET 99407		ALH 84025		EET 99402				EET 99407		EET 99407	
	ave	std	ave	std	ave	std	ave	std	ave	std	ave	std	ave	std	ave	std	ave	std	ave	std
n*	5		3		5		6		5		5		7		5		5		5	
SiO_2	37.12	0.05	36.8	0.2	36.49	0.04	36.8	0.2	36.56	0.09	53.2	0.1	52.9	0.1	52.9	0.2	53.1	0.2	57.2	0.2
TiO_2	-	-	-	-	-	-	-	-	-	-	0.159	0.002	0.135	0.006	0.131	0.004	0.135	0.002	-	-
Al_2O_3	-	-	-	-	-	-	-	-	-	-	0.721	0.007	1.10	0.01	1.03	0.02	1.065	0.006	27.22	0.05
Cr_2O_3	0.046	0.004	0.045	0.005	0.018	0.004	0.028	0.005	0.015	0.005	0.96	0.02	0.850	0.009	0.77	0.01	0.81	0.02	-	-
FeO	29.47	0.06	29.5	0.1	30.9	0.1	30.7	0.1	31.0	0.1	7.00	0.06	7.05	0.02	6.0	0.1	6.6	0.1	0.10	0.03
MnO	0.423	0.004	0.409	0.003	0.402	0.007	0.401	0.006	0.404	0.004	0.219	0.003	0.183	0.004	0.146	0.003	0.160	0.007	-	-
MgO	32.87	0.06	32.45	0.01	31.1	0.1	31.1	0.3	31.17	0.07	15.89	0.06	15.36	0.09	15.19	0.04	15.41	0.03	0.029	0.005
CaO	0.098	0.005	0.11	0.01	0.105	0.008	0.26	0.02	0.100	0.003	21.0	0.2	21.75	0.04	22.88	0.08	22.4	0.1	8.3	0.1
NiO	0.020	0.006	0.32	0.05	0.014	0.004	-	-	0.017	0.007	-	-	-	-	-	-	-	-	-	-
Na_2O	-	-	-	-	-	-	-	-	-	-	0.483	0.009	0.351	0.008	0.370	0.008	0.379	0.007	6.88	0.04
K_2O	-	-	-	-	-	-	-	-	-	-	-	-	-	-	-	-	-	-	0.038	0.005
sum	100.047		99.634		99.029		99.289		99.266		99.632		99.679		99.417		100.059		99.767	
*molar Fe/Mn, 100*Mg/(Mg+Fe) and mole percent mineral end members.*																				
Fe/Mn	68.8		71.2		75.8		75.6		75.7		31.6		38.0		40.6		40.7			
mg#	66.5		66.2		64.3		64.4		64.2		80.2		79.5		81.9		80.6			
Wo,Or											43.2		44.7		47.0		45.7		0.2	
En,Ab											45.6		44.0		43.4		43.8		59.9	
Fs,An											11.2		11.3		9.6		10.5		39.9	
atoms per formula unit																				
Si	1.0004		0.9985		1.0021		1.0062		1.0019		1.9737		1.9652		1.9671		1.9642		2.5811	
Ti	-		-		-		-		-		0.0044		0.0038		0.0037		0.0038		-	
Al	-		-		-		-		-		0.0309		0.0472		0.0443		0.0455		1.4199	
Cr	0.0010		0.0010		0.0004		0.0006		0.0003		0.0282		0.0250		0.0226		0.0237		-	
Fe	0.6642		0.6694		0.7086		0.7020		0.7097		0.2172		0.2190		0.1866		0.2042		0.0038	
Mn	0.0097		0.0094		0.0094		0.0093		0.0094		0.0069		0.0058		0.0046		0.0050		-	
Mg	1.3206		1.3125		1.2738		1.2677		1.2733		0.8788		0.8506		0.8420		0.8497		0.0020	
Ca	0.0028		0.0032		0.0031		0.0076		0.0029		0.8348		0.8658		0.9116		0.8878		0.4013	
Ni	0.0004		0.0070		0.0003		-		0.0004		-		-		-		-		-	
Na	-		-		-		-		-		0.0347		0.0253		0.0267		0.0272		0.6020	
K	-		-		-		-		-		-		-		-		-		0.0022	
sum	2.9991		3.0010		2.9977		2.9934		2.9979		4.0096		4.0077		4.0092		4.0111		5.0123	

* Number of analyses averaged.

Table 3. Average compositions for representative chromite grains from ALH 84025, EET 99402 and EET 99407.

	ALH 84025				EET 99402				EET 99407					
	ave	std	ave	std	ave	std	ave	std	ave	std	ave	std	ave	std
n*	6		10		6		6		4		7		10	
TiO_2	1.289	0.007	1.32	0.01	0.966	0.006	1.00	0.01	0.992	0.007	0.96	0.01	1.01	0.01
Cr_2O_3	59.8	0.2	60.6	0.1	52.58	0.09	53.7	0.2	52.2	0.5	53.10	0.07	53.0	0.3
Al_2O_3	7.45	0.03	7.42	0.04	13.69	0.06	12.88	0.09	13.8	0.2	13.4	0.1	13.3	0.1
V_2O_3	0.409	0.004	0.409	0.003	0.370	0.004	0.359	0.005	0.375	0.007	0.371	0.003	0.350	0.004
FeO	28.79	0.08	27.3	0.2	28.20	0.09	27.7	0.1	28.6	0.2	28.08	0.08	27.1	0.1
MnO	0.338	0.006	0.320	0.009	0.289	0.007	0.280	0.003	0.292	0.006	0.289	0.006	0.281	0.007
MgO	2.85	0.02	3.9	0.1	4.29	0.03	4.53	0.02	4.1	0.1	4.37	0.03	4.65	0.02
ZnO	0.46	0.01	0.41	0.01	0.02	0.01	0.019	0.009	0.019	0.003	0.015	0.005	0.400	0.010
sum	101.386		101.679		100.405		100.468		100.378		100.585		100.091	
*molar Fe/Mn, 100*Mg/(Mg+Fe), 100*Cr/(Cr+Al) and spinel end members*														
Fe/Mn	84.1		84.2		96.3		97.7		96.7		95.9		95.2	
mg#	15.0		20.3		21.3		22.6		20.3		21.7		23.4	
cr#	84.3		84.6		72.0		73.7		71.7		72.7		72.8	
Cm	68.5		63.8		54.5		54.7		54.9		54.7		53.4	
Mc	13.1		17.8		15.7		17.1		15.0		16.2		17.5	
Hc	12.7		11.7		21.2		19.6		21.7		20.6		20.0	
Sp	2.4		3.3		6.1		6.1		5.9		6.1		6.5	
Uv	3.3		3.4		2.5		2.5		2.5		2.4		2.6	
atoms per formula unit														
Ti	0.0336		0.0340		0.0245		0.0254		0.0252		0.0243		0.0257	
Cr	1.6378		1.6425		1.4009		1.4324		1.3927		1.4135		1.4152	
Al	0.3042		0.2998		0.5438		0.5122		0.5489		0.5318		0.5294	
V	0.0114		0.0112		0.0100		0.0097		0.0101		0.0100		0.0095	
Fe	0.8340		0.7827		0.7948		0.7816		0.8071		0.7906		0.7654	
Mn	0.0099		0.0093		0.0082		0.0080		0.0083		0.0082		0.0080	
Mg	0.1471		0.1992		0.2155		0.2278		0.2062		0.2193		0.2340	
Zn	0.0118		0.0104		0.0005		0.0005		0.0005		0.0004		0.0100	
sum	2.9898		2.9891		2.9982		2.9976		2.9990		2.9981		2.9972	

* Number of analyses averaged.

Table 4. Average compositions for representative troilite and metal grains from ALH 84025.

	troilite						metal					
	ave	std	ave	std	ave	std	ave	std	ave	std	ave	std
n*	5		5		5		5		5		5	
Fe	63.0	0.1	62.70	0.04	62.7	0.2	69.9	0.5	69.0	0.1	66.0	0.3
Ni	0.040	0.006	0.39	0.04	0.62	0.06	28.87	0.03	29.7	0.1	31.40	0.04
Co	0.028	0.004	0.06	0.02	0.058	0.007	1.620	0.002	1.575	0.007	1.670	0.008
Cr	0.054	0.003	0.054	0.003	0.055	0.003	-	-	-	-	-	-
S	36.9	0.1	36.4	0.1	36.38	0.09	-	-	-	-	-	-
sum	100.026		99.601		99.831		100.457		100.334		99.094	
	atom percent											
Fe	49.4		49.5		49.5		70.7		69.9		67.7	
Ni	0.030		0.29		0.47		27.77		28.6		30.65	
Co	0.021		0.04		0.043		1.552		1.512		1.624	
Cr	0.046		0.046		0.047		-		-		-	
S	50.5		50.1		50.0		-		-		-	

* Number of analyses averaged.

Table 5. Select major, minor and trace element contents of EET 99402 and EET 99407*.

		EET 99402,12	EET 99402,19	EET 99402,22‡	EET 99407,6
mass (mg)†		52.80	53.41		53.39
Na	mg/g	2.562 ± 0.016	2.501 ± 0.013	*3.3*	3.640 ± 0.019
Mg	*mg/g*	*171*	*174*	*172*	*169*
Al	*mg/g*	*8.1*	*7.6*	*9.9*	*10.8*
Si	*mg/g*	*175*	*175*	*179*	*177*
Ca	mg/g	10.8 ± 1.7	8.6 ± 1.2	*12*	10.2 ± 1.3
Sc	µg/g	8.08 ± 0.03	7.14 ± 0.03		6.93 ± 0.03
Cr	mg/g	5.27 ± 0.03	3.174 ± 0.015	*4.1*	3.086 ± 0.014
Fe	mg/g	225.0 ± 0.8	227.7 ± 0.8	*219*	223.3 ± 0.8
Co	µg/g	202.5 ± 0.8	204.5 ± 0.8		208.7 ± 0.8
Ni	µg/g	686 ± 17	702 ± 16		796 ± 17
Zn	µg/g	21 ± 4	22 ± 3		16.2 ± 1.9
Se	µg/g	1.43 ± 0.13	1.32 ± 0.11		1.4 ± 0.12
La	ng/g	=36	=20		=20
Sm	ng/g	8.7 ± 1.6	7.4 ± 1.4		7.5 ± 1.2
Eu	ng/g	38 ± 3	33 ± 2		48 ± 3
Yb	ng/g	62 ± 16	48 ± 16		50 ± 15
Lu	ng/g	=15	=16		7 ± 3
Ir	ng/g	32.4 ± 1.1	29.6 ± 1.0		33.0 ± 1.1
Au	ng/g	2.6 ± 0.4	1.9 ± 0.4		2.9 ± 0.4

* Determined by INAA. Uncertainties are ±1s, upper limits are 2s. Contents of Mg, Al and Si were calculated from the INAA and mineral composition data. See text.

† Mass of sample analyzed. The samples are splits of homogenized powders of larger samples. See text.

‡ Major element contents were calculated from element maps of thin section and mineral composition data. See text.

Figure 1. Photomicrographs of general textural features of EET 99407 and ALH 84025. Note the general dusty appearance of grains in EET 99407 compared to the more transparent grains in ALH 84025. Twinned grains are augite, not plagioclase. Plagioclase patches in EET 99407 are composed of numerous grains a few μm in size. The labeled grain contains a rounded vesicle. Labels are; crm – chromite, cpx – high-Ca pyroxene, met – metal, oliv – olivine, plg – plagioclase, troi – troilite.

Figure 2. CaO vs. Cr_2O_3 in brachinite olivine compared to those of acapulcoite-lodranite clan meteorites, L7 chondrite LEW 88663 and L chondrite impact-melt PAT 91501. High CaO contents of olivine are characteristic of high temperature, igneous grains. LEW 88663 is an example of equilibrated ordinary chondrites. The major and minor element compositions of its minerals match those of L5-6 chondrites – see Brearley and Jones (1998), Mittlefehldt and Lindstrom (2001). Brachina data from Smith et al. (1983). Acapulcoite-lodranite data from Mittlefehldt et al. (1996) and Mittlefehldt, unpublished. LEW 88663 and PAT 91501 data from Mittlefehldt and Lindstrom (2001).

Figure 3. TiO_2 vs. Al_2O_3 and Na_2O vs. Cr_2O_3 in brachinite high-Ca pyroxene compared to those of acapulcoite-lodranite clan meteorites, L7 chondrite LEW 88663, and L chondrite impact-melt PAT 91501. Data sources as in Fig. 2, plus additional Brachina data from Nehru et al. (1983).

Figure 4. Plagioclase compositions of EET 9940n compared to those of Brachina, acapulcoites L7 chondrite LEW 88663, and L chondrite impact-melt PAT 91501. Brachina data are from Nehru et al. (1983). Acapulcoite, LEW 88663 and PAT 91501 data are from sources given in Fig. 2.

Figure 5. Chrome-rich spinel compositions of ALH 84025 and EET 9940n compared to those of Brachina, acapulcoite-lodranite clan meteorites, L7 chondrite LEW 88663, and L chondrite impact-melt PAT 91501. The curved arrow shows the zoning trend for PAT 91501 spinels (Mittlefehldt and Lindstrom, 2001). EET 9940n spinels are Al-rich and, with one exception, very Zn-poor compared to those of other brachinites. Brachina data are from Nehru et al. (1983). Acapulcoite-lodranite, LEW 88663 and PAT 91501 data are from sources listed in Fig. 2.

Figure 6. Equal area stereonet plots of X, Y, and Z light vibration directions for olivine in Antarctic brachinites. Contour lines equal 2, 4, and 6% in 1% of area. Fifty grains measured in each meteorite. (a) EET 99407,9: "l " in Y=c is the lineation (vertical), maximum equals 14% in 1% of area. (b) ALH 84025,6: Y=c lineation denoted as double headed arrow labeled "l "(near horizontal, plunging to east), maximum equals 8% in 1% of area.

Figure 7. Equal area stereonet plots of X, Y, and Z light vibration directions of olivine in ALH 84025,6 for (a) elongate (high aspect ratio) and (b) equant (low aspect ratio) grains; 25 grains measured for each type. Contours represent 2%, 4% and 6% in 1% of area. Patterns are virtually identical and mimic patterns shown in Fig. 6b.

Figure 8. Rare earth element patterns for brachinites compared to those of the acapulcoite ALHA81261 and lodranite MAC 88177. Data are from Mittlefehldt et al. (1996) – ALHA81261, MAC 88177; Nehru et al. (1983) – Brachina; Warren and Kallemeyn (1989) – ALH 84025.

Figure 9. Siderophile element and Se diagram for brachinites compared to select acapulcoite-lodranite clan meteorites. Brachinite data are from Nehru et al. (1983) – Brachina; Swindle et al. (1998) – Eagles Nest; Warren and Kallemeyn (1989) – ALH 84025. Acapulcoite-lodranite samples are averages of data from Mittlefehldt et al. (1996), Rubin et al. (2002), Weigel et al. (1999) and Zipfel and Palme (1993).

Figure 10. ^{39}Ar-^{40}Ar ages (rectangles, left scale) and K/Ca ratios (stepped line, right scale) as a function of cumulative release of ^{39}Ar for stepwise temperature extractions of a whole rock sample of EET 99402. Potassium and Ca concentrations are also given.

Figure 11. ^{39}Ar-^{40}Ar ages (rectangles, left scale) and K/Ca ratios (stepped line, right scale) as a function of cumulative release of ^{39}Ar for stepwise temperature extractions of a whole rock sample of Brachina. Potassium and Ca concentrations are also given.

Figure 12. Plot of ^{129}Xe/^{132}Xe vs. ^{128}Xe/^{132}Xe for stepwise temperature degassing of Brachina. Five extractions above 1100 ^{o}C (solid points) define a linear correlation.

Figure 13. Photomicrographs of terrestrial and meteoritic metamorphic tectonites and igneous cumulates showing varying degrees of mineral elongation preferred orientation. All

photos were contrast-enhanced to accentuate fabrics. Straight lines represent approximate lineation trends. (a) Dreiser Weiher tectonite (Fig. 6A in Mercier and Nicolas, 1975); (b) Kenna ureilite (Berkley et al., 1976), a partial melt residue and tectonite; (c) Governador Valladares nakhlite, martian cumulate clinopyroxenite, (d) Theos Flow, ultrabasic cumulate lava flow; (e) ALH 84025,6 brachinite.

Figure 14. Olivine and pyroxene compositional data and bulk rock siderophile element ratios for brachinites giving evidence for differences in oxidation state, and probable partial oxidation of Co; see text. Literature data from Nehru et al. (1983), Smith et al. (1983), Swindle et al. (1998), Warren and Kallemeyn (1989) and D. Kring, personal communication. Note that D. Kring provided two distinct olivine compositions for Eagles Nest – both are plotted.

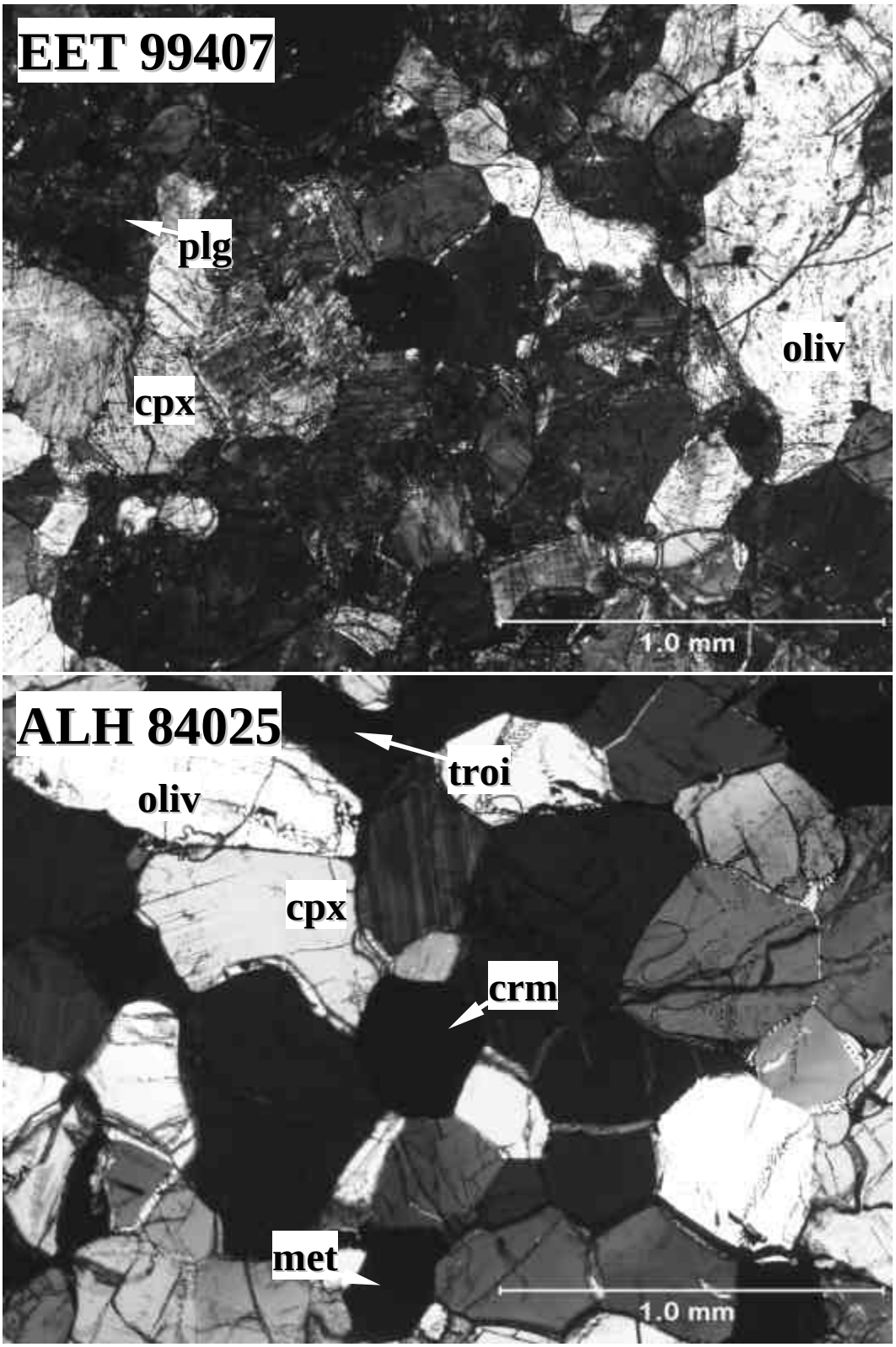
EET 99407
plg
oliv
cpx
1.0 mm
ALH 84025
troi
oliv
cpx
crm
met
1.0 mm

Figure 1

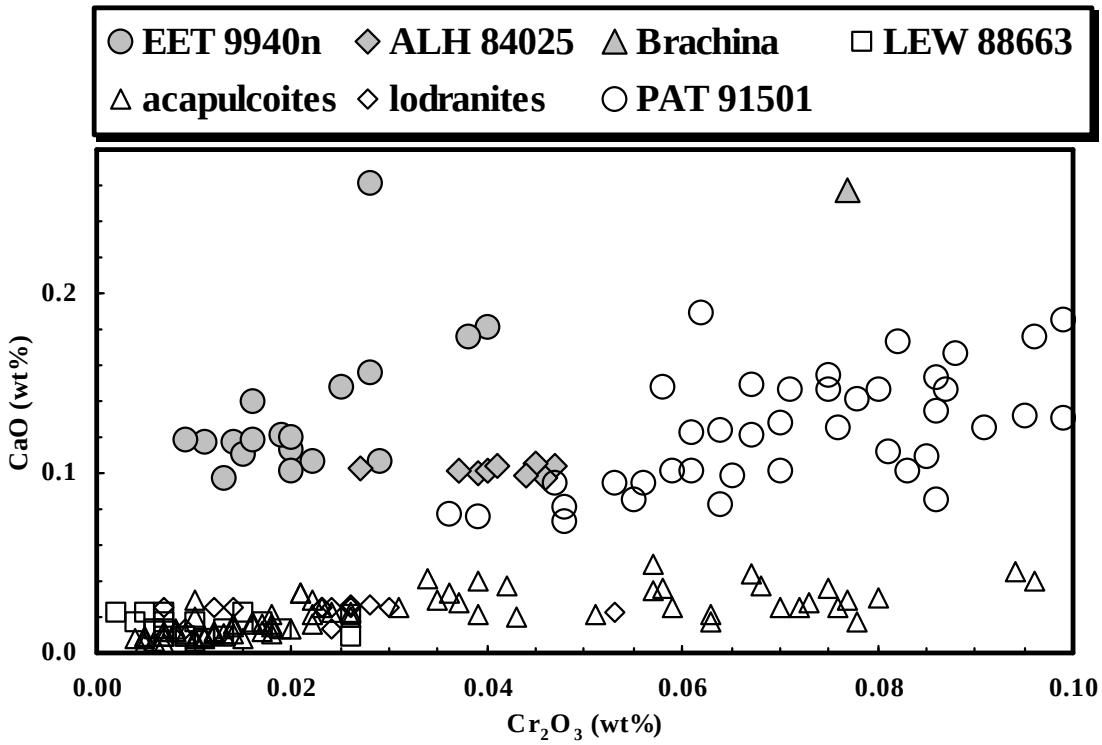
EET 9940n
ALH 84025
Brachina
LEW 88663
acapulcoites
lodranites
PAT 91501
CaO (wt%)
0.0
0.1
0.2
0.00
0.02
0.04
0.06
0.08
0.10
Cr2O3 (wt%)

Figure 2

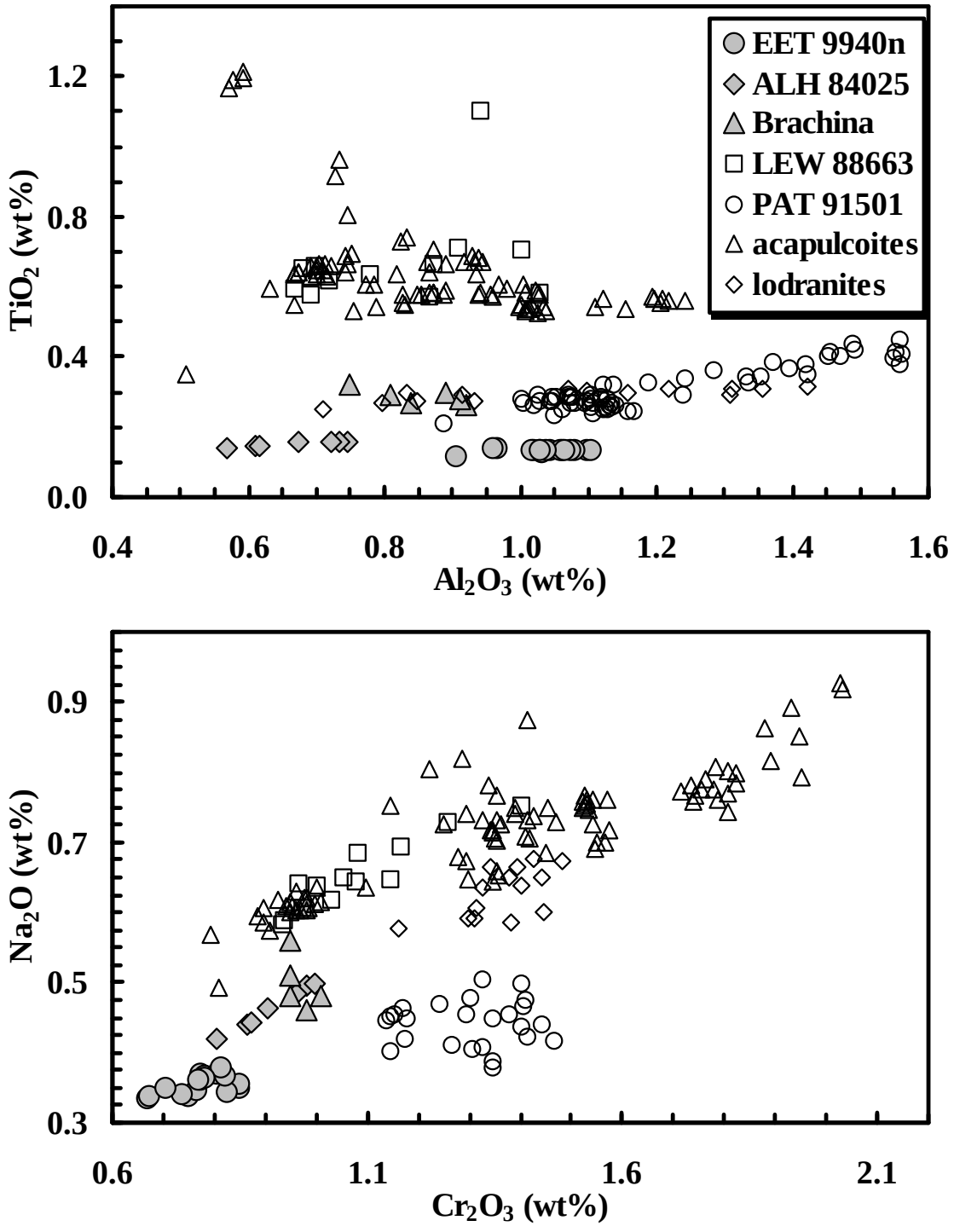
EET 9940n
ALH 84025
Brachina
LEW 88663
PAT 91501
acapulcoites
lodranites
TiO2 (wt%)
Al2O3 (wt%)
Na2O (wt%)
Cr2O3 (wt%)
0.0
0.4
0.8
1.2
0.4
0.6
0.8
1.0
1.2
1.4
1.6
0.3
0.5
0.7
0.9
0.6
1.1
1.6
2.1

Figure 3

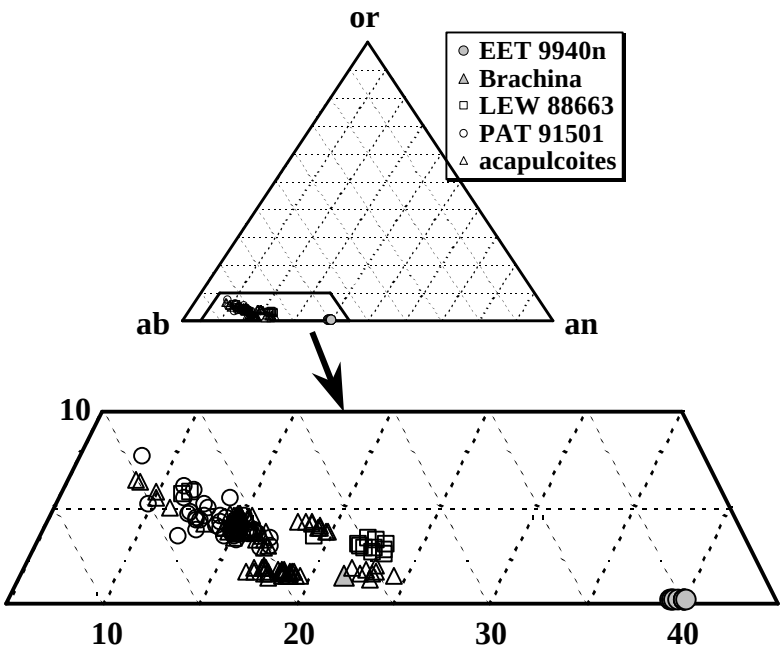
or
EET 9940n
Brachina
LEW 88663
PAT 91501
acapulcoites
ab
an
10
10
20
30
40

Figure 4

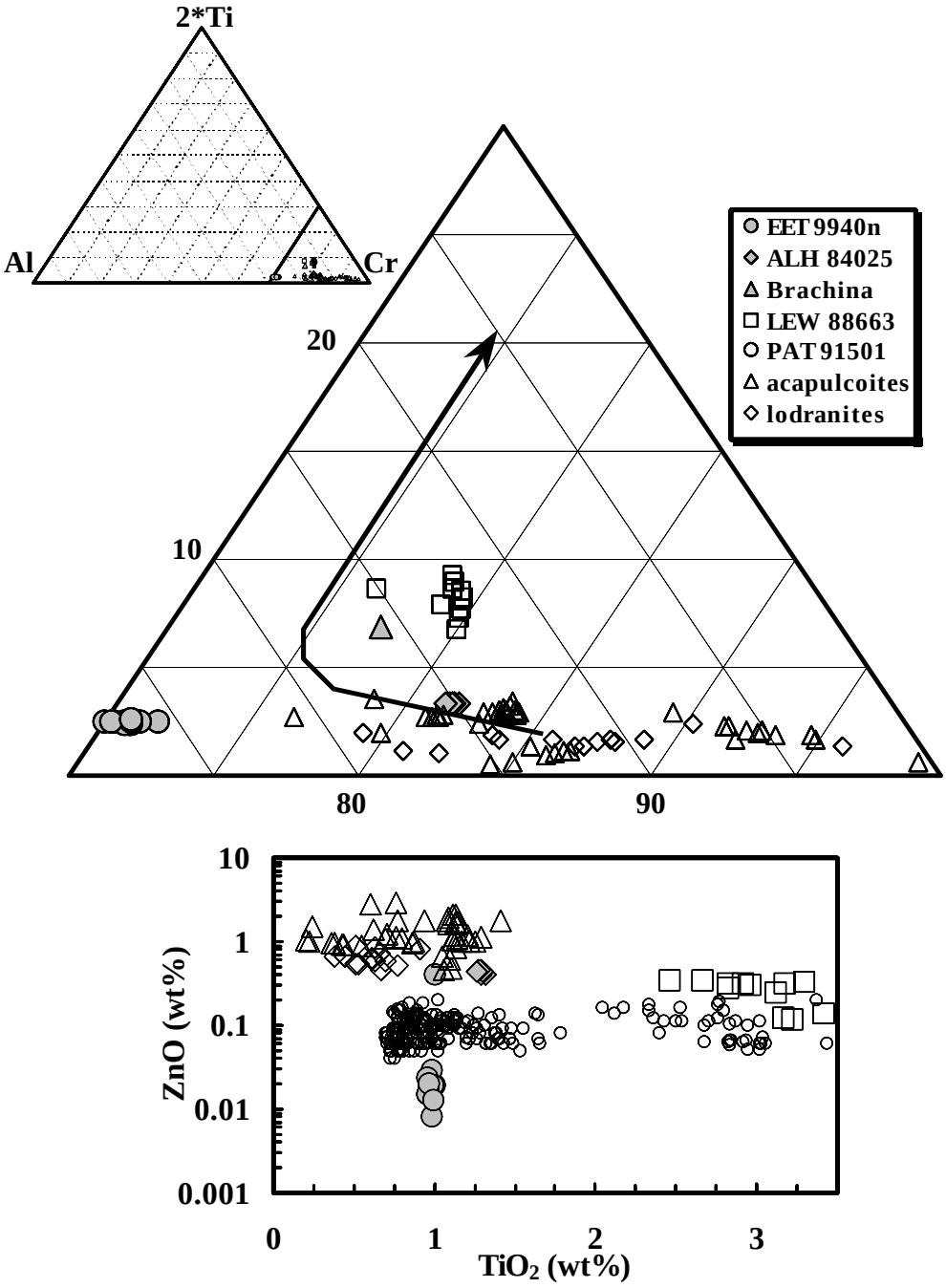
2*Ti
Al
Cr
20
10
80
90
EET 9940n
ALH 84025
Brachina
LEW 88663
PAT 91501
acapulcoites
lodranites
10
1
0.1
0.01
0.001
ZnO (wt%)
0
1
2
3
TiO2 (wt%)

Figure 5

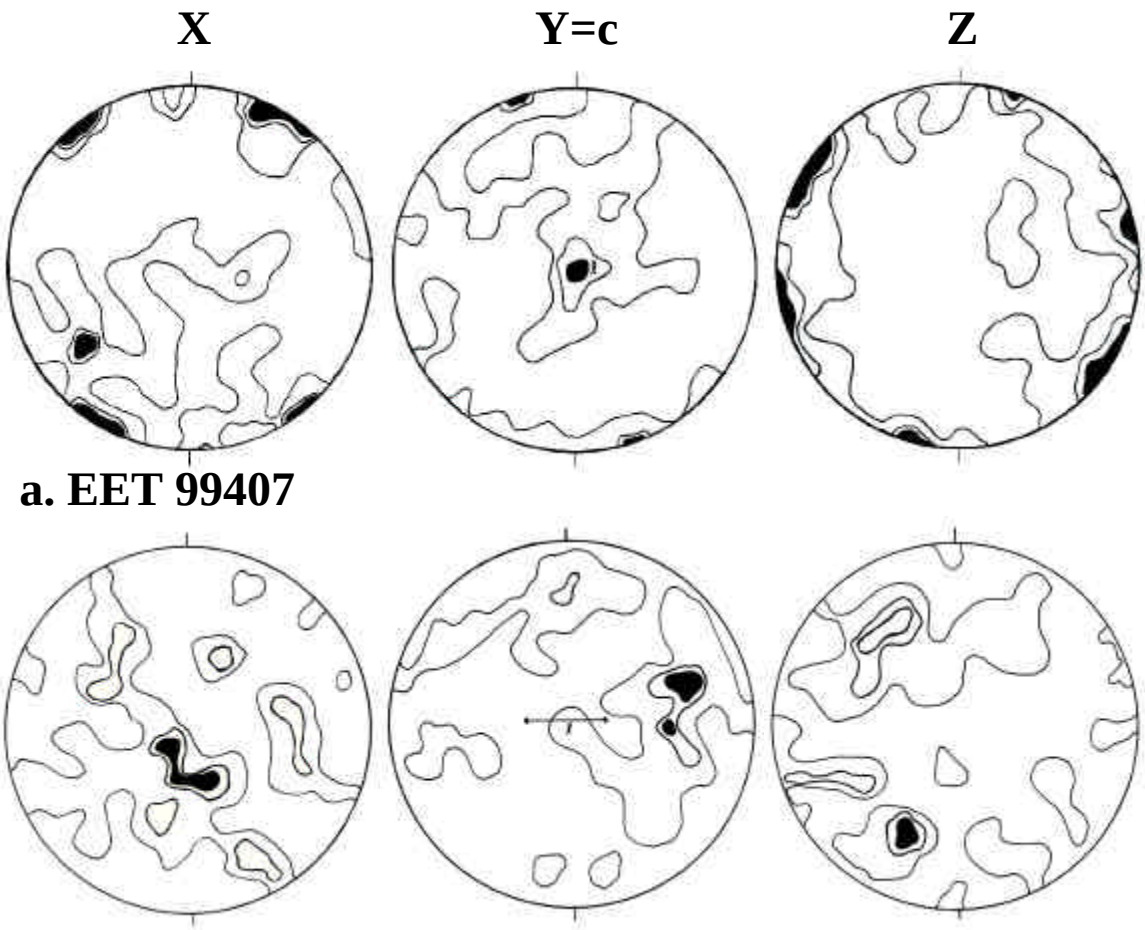

Figure 6

ALH 84025

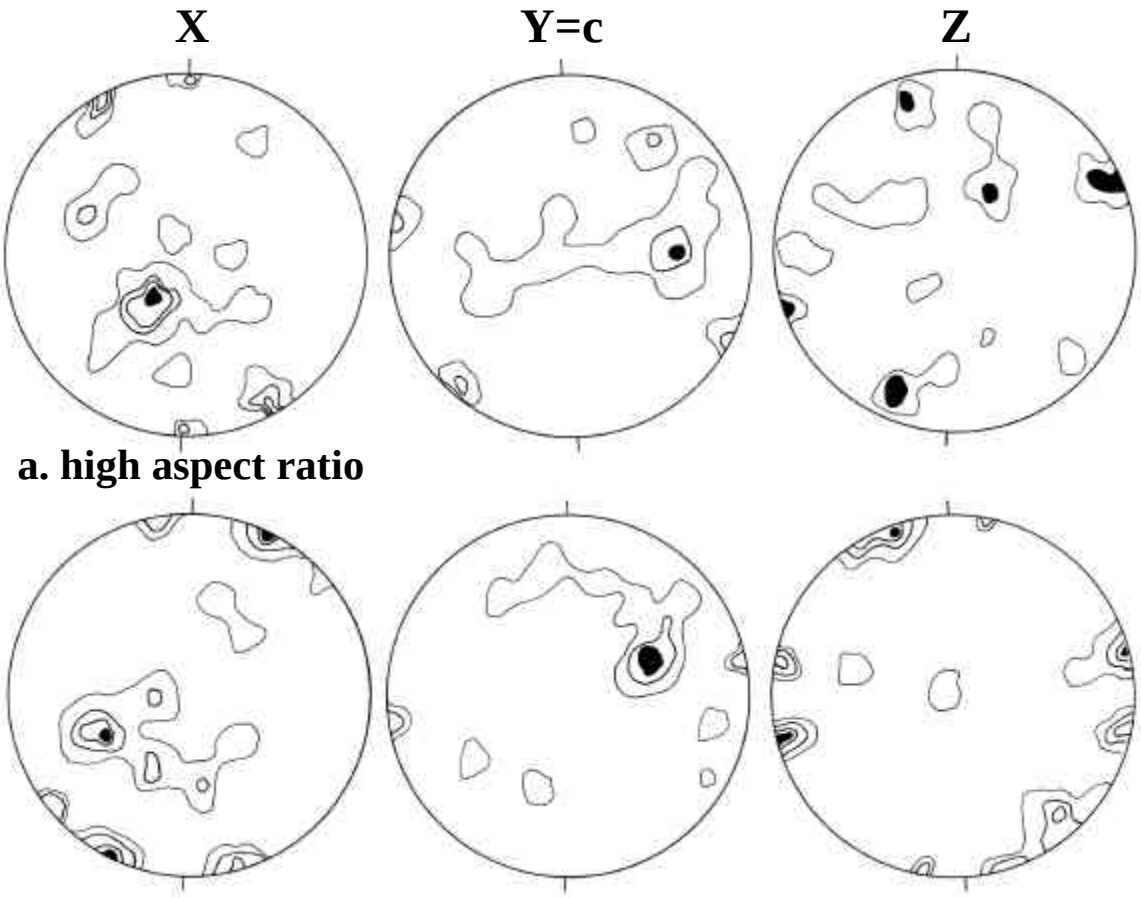

Figure 7

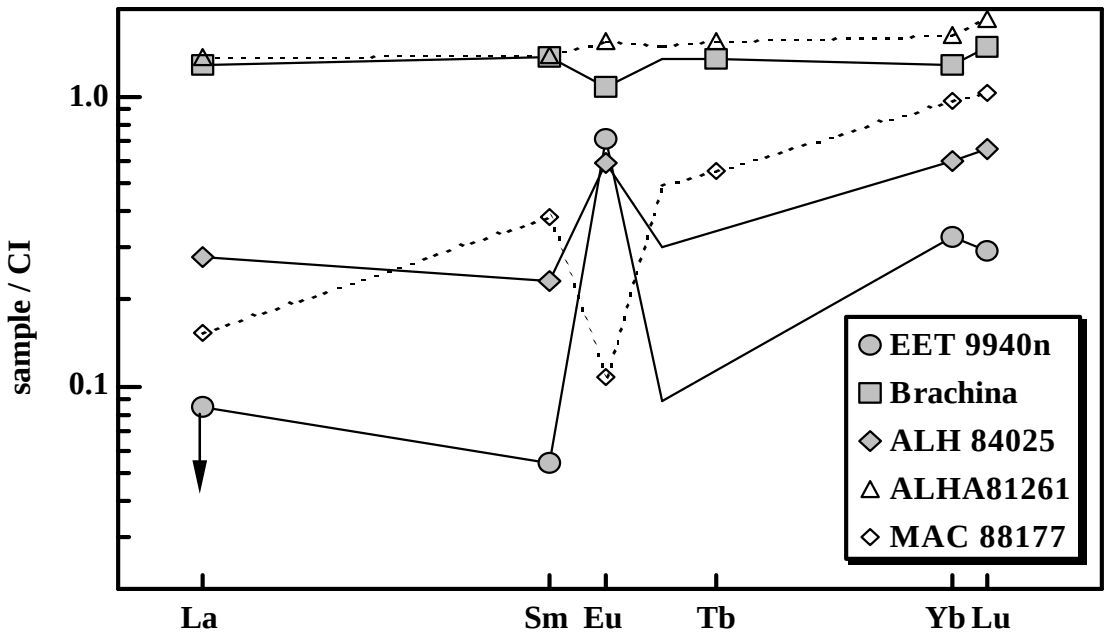
1.0
0.1
sample / CI
La
Sm
Eu
Tb
Yb
Lu
EET 9940n
Brachina
ALH 84025
ALHA81261
MAC 88177

Figure 8

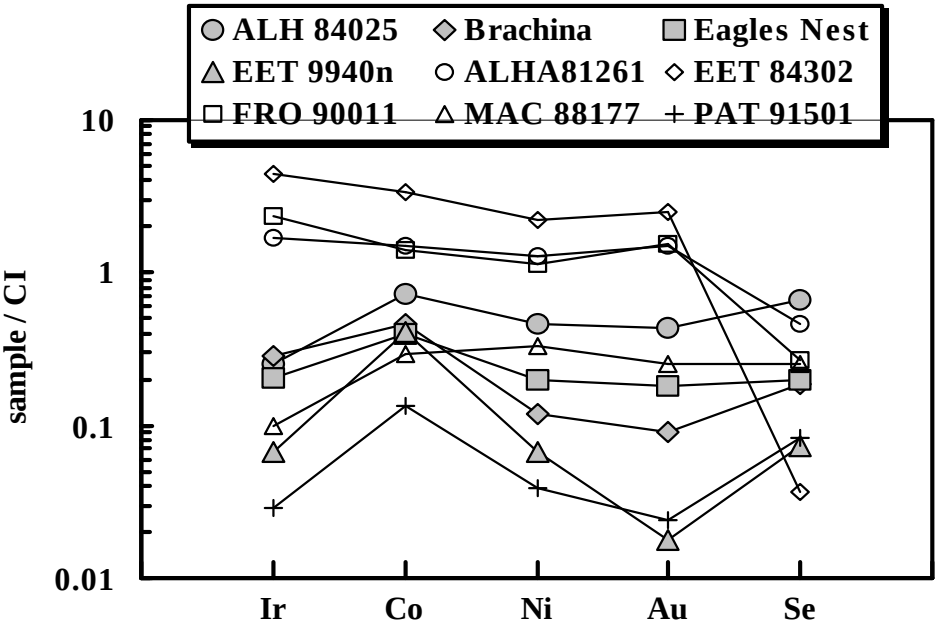
ALH 84025
Brachina
Eagles Nest
EET 9940n
ALHA81261
EET 84302
FRO 90011
MAC 88177
PAT 91501
10
1
0.1
0.01
sample / CI
Ir
Co
Ni
Au
Se

Figure 9

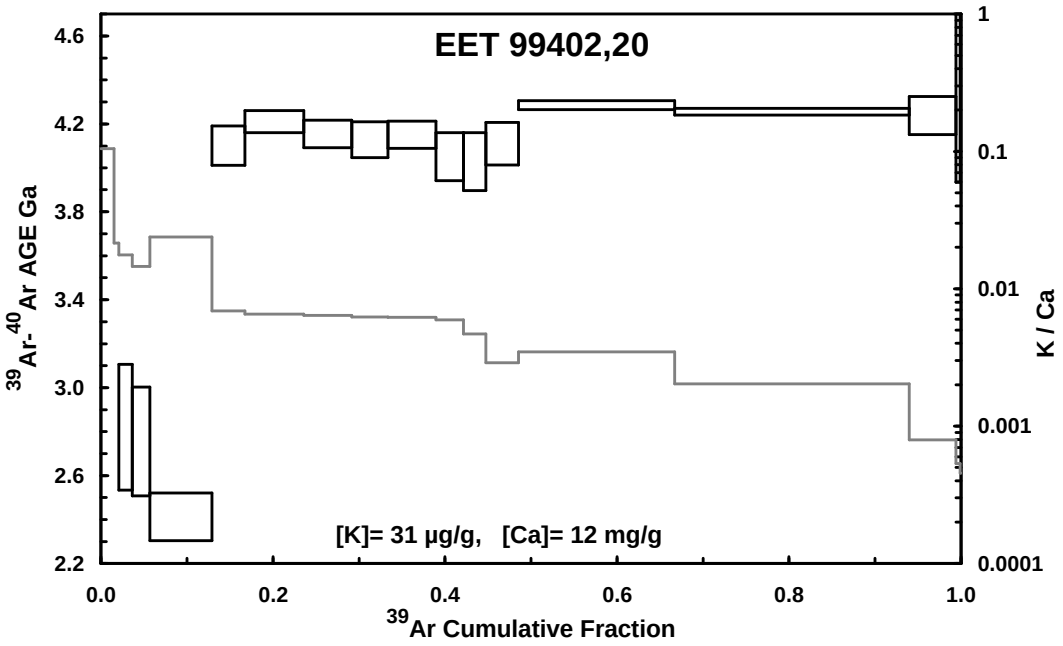
EET 99402,20
4.6
4.2
3.8
3.4
3.0
2.6
2.2
39Ar-40Ar AGE Ga
1
0.1
0.01
0.001
0.0001
K / Ca
[K]= 31 µg/g, [Ca]= 12 mg/g
0.0
0.2
0.4
0.6
0.8
1.0
39Ar Cumulative Fraction

Figure 10

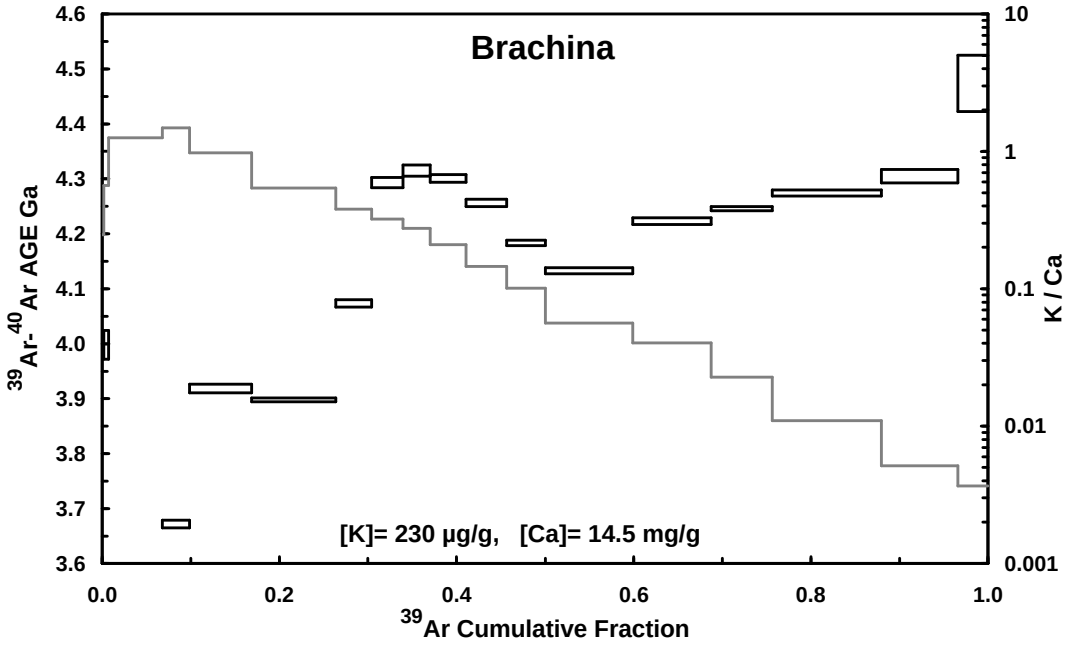
Brachina
[K]= 230 µg/g, [Ca]= 14.5 mg/g
39Ar- 40Ar AGE Ga
K / Ca
39Ar Cumulative Fraction
4.6
4.5
4.4
4.3
4.2
4.1
4.0
3.9
3.8
3.7
3.6
10
1
0.1
0.01
0.001
0.0
0.2
0.4
0.6
0.8
1.0

Figure 11

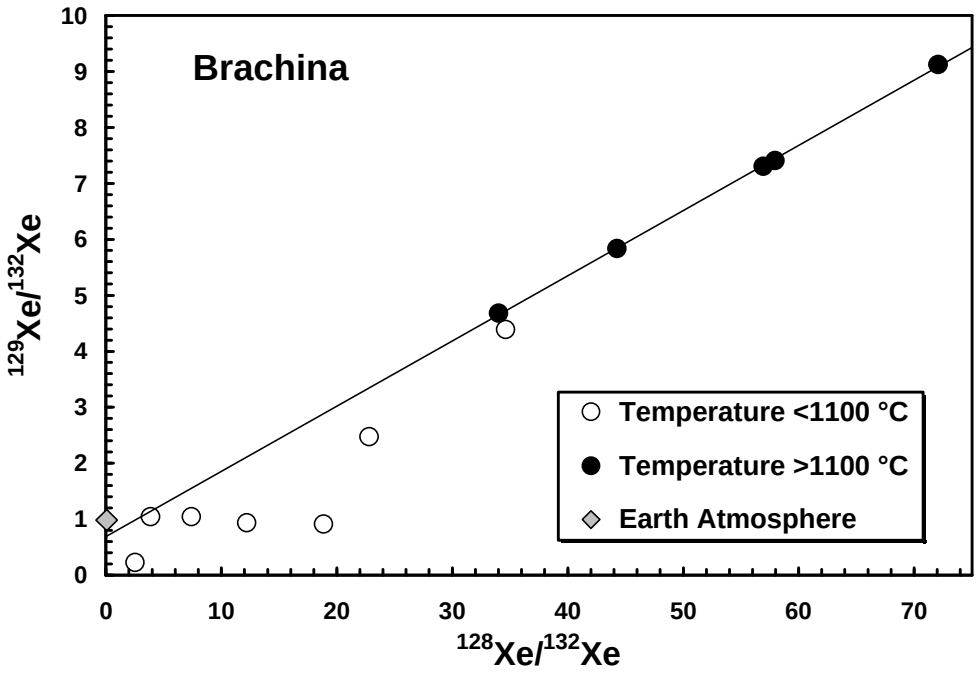
Brachina
$^{129}Xe/^{132}Xe$
$^{128}Xe/^{132}Xe$
0
1
2
3
4
5
6
7
8
9
10
0
10
20
30
40
50
60
70
Temperature <1100 °C
Temperature >1100 °C
Earth Atmosphere

Figure 12

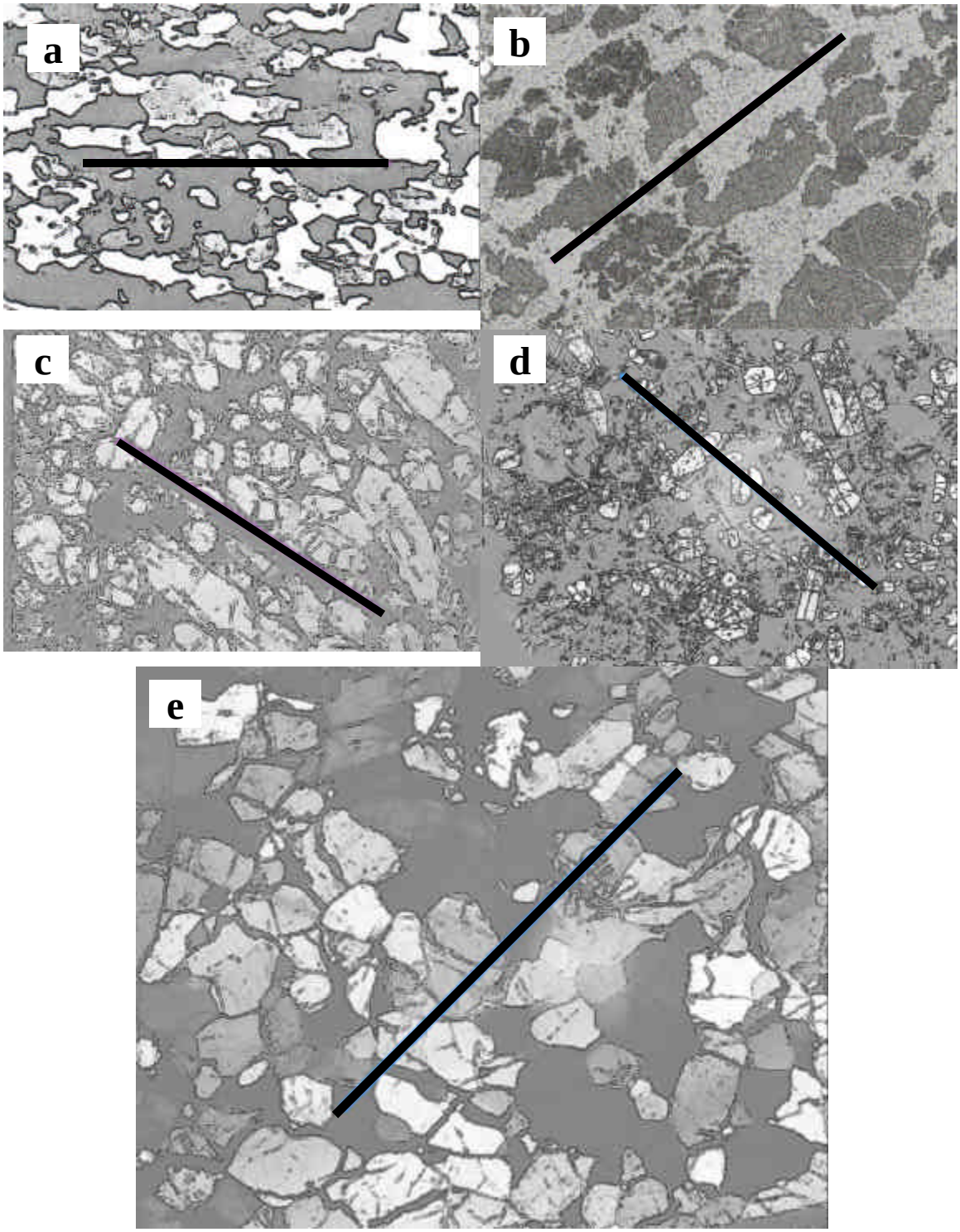

Figure 13

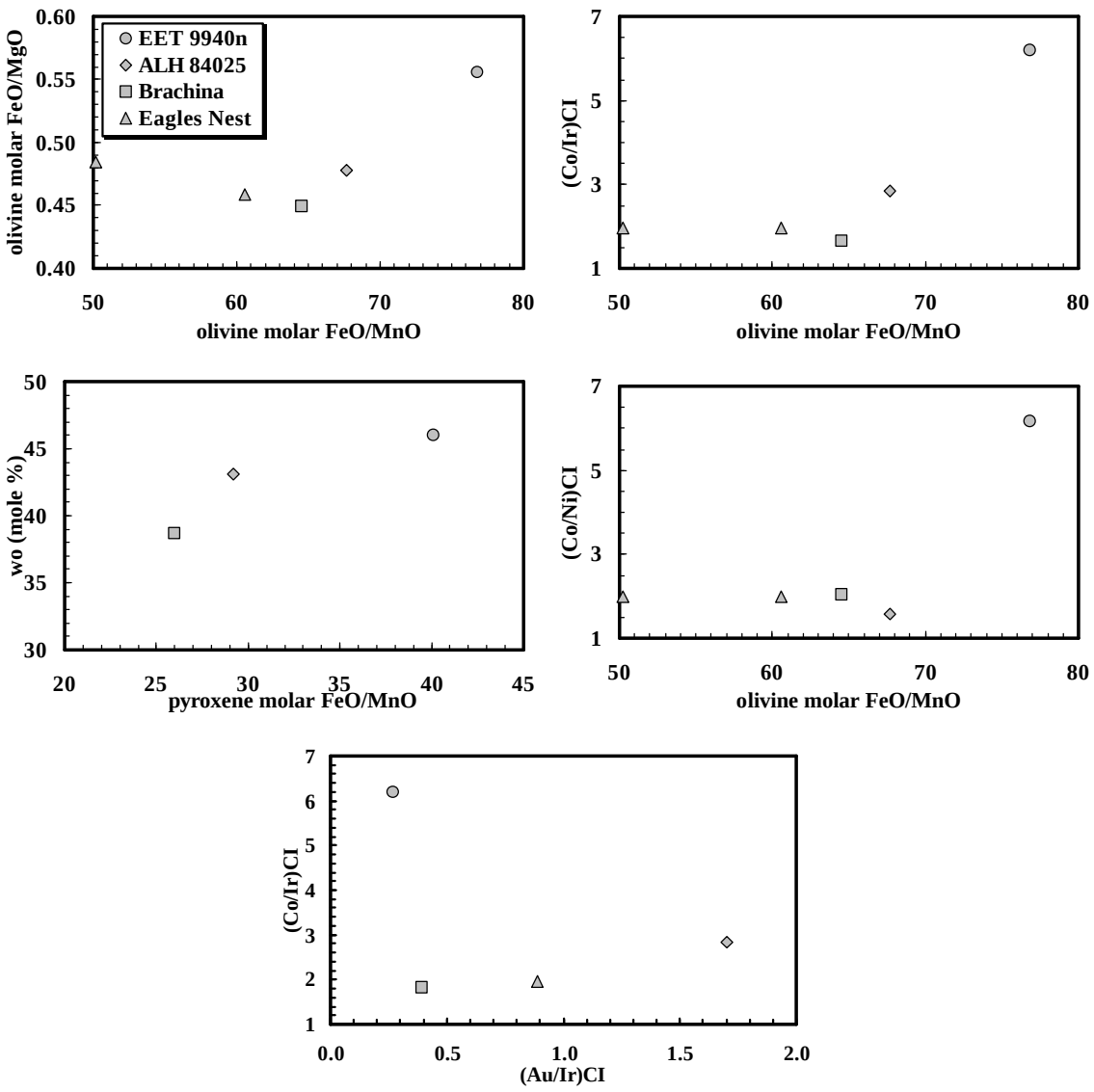
EET 9940n
ALH 84025
Brachina
Eagles Nest
olivine molar FeO/MgO
olivine molar FeO/MnO
(Co/Ir)CI
olivine molar FeO/MnO
wo (mole %)
pyroxene molar FeO/MnO
(Co/Ni)CI
olivine molar FeO/MnO
(Co/Ir)CI
(Au/Ir)CI

Figure 14